

Investigation of the Planar Near-Field Measurement of a  
Reflector Antenna and a Reflector-plus-Splash Plate Antenna  
System at X-band

October 31, 1996

DTIC QUALITY INSPECTED 2

Prepared by

PAUL R. ROUSSEAU  
Electromagnetic Techniques Department  
Communication Systems Subdivision  
Electronic Systems Division

Prepared for

SPACE AND MISSILE SYSTEMS CENTER  
AIR FORCE MATERIEL COMMAND  
2430 E. El Segundo Boulevard  
Los Angeles Air Force Base, CA 90245

Contract No. F04701-93-C-0094

Engineering and Technology Group

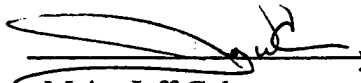
APPROVED FOR PUBLIC RELEASE; DISTRIBUTION UNLIMITED.

19970409 079

This report was submitted by The Aerospace Corporation, El Segundo, CA 90245-4691, under Contract No. F04701-93-C-0094 with the Space and Missile Systems Center, P. O. Box 92960, Los Angeles, CA 90009-2960. It was reviewed and approved for The Aerospace Corporation by K. M. Soo Hoo, Principal Director, Communication Systems Subdivision . The project officer is Major Jeff Cole.

This report has been reviewed by the Public Affairs Office (PAS) and is releasable to the National Technical Information Service (NTIS). At NTIS, it will be available to the general public, including foreign nationals.

This technical report has been reviewed and is approved for publication. Publication of this report does not constitute Air Force approval of the report's findings or conclusions. It is published only for the exchange and stimulation of ideas.

  
Major Jeff Cole  
Project Officer

# REPORT DOCUMENTATION PAGE

Form Approved  
OMB No. 0704-0188

Public reporting burden for this collection of information is estimated to average 1 hour per response, including the time for reviewing instructions, searching existing data sources, gathering and maintaining the data needed, and completing and reviewing the collection of information. Send comments regarding this burden estimate or any other aspect of this collection of information, including suggestions for reducing this burden, to Washington Headquarters Services, Directorate for Information Operations and Reports, 1215 Jefferson Davis Highway, Suite 1204, Arlington, VA 22202-4302, and to the Office of Management and Budget, Paperwork Reduction Project (0704-0188), Washington, DC 20503.

1. AGENCY USE ONLY (Leave blank)	2. REPORT DATE October 31, 1996	3. REPORT TYPE AND DATES COVERED	
4. TITLE AND SUBTITLE Investigation of the Planar Near-Field Measurement of a Reflector Antenna and a Reflector-plus-Splash Plate Antenna System at X-band		5. FUNDING NUMBERS  F04701-93-C-0094	
6. AUTHOR(S)  Paul R. Rousseau		8. PERFORMING ORGANIZATION REPORT NUMBER  TR-97(8560)-1	
7. PERFORMING ORGANIZATION NAME(S) AND ADDRESS(ES) The Aerospace Corporation 2350 E. El Segundo Blvd. El Segundo, CA 90245-4691			
9. SPONSORING/MONITORING AGENCY NAME(S) AND ADDRESS(ES) Space and Missile Systems Center Air Force Materiel Command 2350 E. El Segundo Blvd. Los Angeles Air Force Base, CA 90245		10. SPONSORING/MONITORING AGENCY REPORT NUMBER  SMC-TR-97-03	
11. SUPPLEMENTARY NOTES			
12a. DISTRIBUTION/AVAILABILITY STATEMENT  Public release; distribution unlimited		12b. DISTRIBUTION CODE	
13. ABSTRACT (Maximum 200 words)  This investigation is motivated by the difficulty of measuring certain multiple reflector antenna systems in a typical near-field range configuration. The three primary objectives of this investigation are: (1) to investigate alternative planar near-field measurement configurations, (2) to support computational simulation studies and (3) to investigate the performance of a particular dish-plus-splash-plate antenna system.			
14. SUBJECT TERMS  Antennas, near-field, measurements		15. NUMBER OF PAGES 58	16. PRICE CODE
17. SECURITY CLASSIFICATION OF REPORT  Unclassified	18. SECURITY CLASSIFICATION OF THIS PAGE  Unclassified	19. SECURITY CLASSIFICATION OF ABSTRACT  Unclassified	20. LIMITATION OF ABSTRACT  Unlimited

# Contents

<b>1</b>	<b>INTRODUCTION</b>	<b>7</b>
<b>2</b>	<b>PLANAR NEAR-FIELD ANTENNA MEASUREMENTS</b>	<b>9</b>
2.1	Antenna Measurement Methods . . . . .	9
2.2	Motivation for Planar Near-field Antenna Measurements . . . . .	10
2.3	Basic Concepts of a Planar Near-field Antenna Measurement . . . . .	10
2.3.1	Near-field to Far-zone Transformation . . . . .	12
2.3.2	Probe Compensation . . . . .	13
2.3.3	Sources of Error . . . . .	13
2.4	Near-field Range Validation and Diagnostics . . . . .	13
<b>3</b>	<b>TILTED ANTENNA CONFIGURATIONS</b>	<b>17</b>
3.1	Significant Sources of Error for a Tilted Antenna Configuration . . . . .	17
3.1.1	Probe Characterization Errors . . . . .	18
3.1.2	Insufficient Sampling . . . . .	18
3.1.3	Scan Area Truncation . . . . .	19
3.1.4	Translational Probe Position Errors . . . . .	19
3.1.5	Room Scattering . . . . .	20
3.1.6	Coordinate System Convention Issues . . . . .	20
3.2	Measurement Results of the Two Foot Dish . . . . .	20
<b>4</b>	<b>DISH-PLUS-SPLASH-PLATE ANTENNA SYSTEM</b>	<b>37</b>
4.1	Measurement Results of Dish-Plus-Splash-Plate Antenna . . . . .	38
4.2	Splash Plate Deformation Study . . . . .	51
4.2.1	Results . . . . .	51
<b>5</b>	<b>CONCLUSION</b>	<b>55</b>

# List of Figures

1	Rule of thumb defining the maximum far-zone angle $\theta_m$ as a function of the AUT aperture size $D$ , scan plane size $L$ and the scan to AUT separation distance $d$ . . . . .	11
2	Definition of $\tau$ ("TAU") angle. For $\tau = 0$ the electric field is polarized in the $x$ direction and for $\tau = 90$ the electric field is polarized in the $y$ direction. . . . .	21
3	The dish is pointed in the same direction as the normal vector of the scan plane. This is the conventional configuration. . . . .	22
4	Comparison of E-plane far-zone pattern obtained from the far-zone range versus the near-field range at 9 GHz. The orientation of the dish in the near-field range is shown in Figure 3. . . . .	23
5	Comparison of H-plane far-zone pattern obtained from the far-zone range versus the near-field range at 9 GHz. The orientation of the dish in the near-field range is shown in Figure 3. . . . .	23
6	Comparison of E-plane far-zone pattern obtained from the far-zone range versus the near-field range at 10 GHz. The orientation of the dish in the near-field range is shown in Figure 3. . . . .	24
7	Comparison of H-plane far-zone pattern obtained from the far-zone range versus the near-field range at 10 GHz. The orientation of the dish in the near-field range is shown in Figure 3. . . . .	24
8	Comparison of E-plane far-zone pattern obtained from the far-zone range versus the near-field range at 11 GHz. The orientation of the dish in the near-field range is shown in Figure 3. . . . .	25
9	Comparison of H-plane far-zone pattern obtained from the far-zone range versus the near-field range at 11 GHz. The orientation of the dish in the near-field range is shown in Figure 3. . . . .	25
10	The dish is pointed at an angle of 45 degrees with respect to the normal vector of the scan plane. . . . .	26
11	Comparison of E-plane far-zone pattern obtained from the near-field range at 10 GHz using the normal configuration in Figure 3 versus the tilted arrangement in Figure 10. . . . .	26
12	Comparison of H-plane far-zone pattern obtained from the near-field range at 10 GHz using the normal configuration in Figure 3 versus the tilted arrangement in Figure 10. . . . .	27

13	Configuration for measuring the far-sidelobes of the dish. The dish is measured once to obtain the sidelobes out to 120 degrees on one side and then rotated 180 degrees about its axis and measured again to obtain the sidelobes out to 120 degrees on the other side. The dish is tilted 45 degrees with respect to the scan plane. . . . .	28
14	Comparison of H-plane far-zone pattern obtained from near-field range versus the far-zone range at 10 GHz. The near-field range configuration shown in 13 was used in order to measure the sidelobe levels out to 120 degrees off of the boresight direction. . . . .	29
15	Comparison of E-plane far-zone pattern obtained from near-field range versus the far-zone range at 10 GHz. The near-field range configuration shown in 13 was used in order to measure the sidelobe levels out to 120 degrees off of the boresight direction. . . . .	29
16	Comparison of H-plane far-zone pattern obtained from near-field range versus the far-zone range at 9 GHz. The near-field range configuration shown in 13 was used in order to measure the sidelobe levels out to 120 degrees off of the boresight direction. . . . .	30
17	Comparison of E-plane far-zone pattern obtained from near-field range versus the far-zone range at 9 GHz. The near-field range configuration shown in 13 was used in order to measure the sidelobe levels out to 120 degrees off of the boresight direction. . . . .	30
18	Comparison of H-plane far-zone pattern obtained from near-field range versus the far-zone range at 11 GHz. The near-field range configuration shown in 13 was used in order to measure the sidelobe levels out to 120 degrees off of the boresight direction. . . . .	31
19	Comparison of E-plane far-zone pattern obtained from near-field range versus the far-zone range at 11 GHz. The near-field range configuration shown in 13 was used in order to measure the sidelobe levels out to 120 degrees off of the boresight direction. . . . .	31
20	Comparison of H-plane far-zone pattern obtained from near-field range versus the far-zone range at 12 GHz. The near-field range configuration shown in 13 was used in order to measure the sidelobe levels out to 120 degrees off of the boresight direction. . . . .	32
21	Comparison of E-plane far-zone pattern obtained from near-field range versus the far-zone range at 12 GHz. The near-field range configuration shown in 13 was used in order to measure the sidelobe levels out to 120 degrees off of the boresight direction. . . . .	32

22	Azimuth-Elevation (AZ-EL) coordinate system used for the far-zone patterns computed from the near-field data. The antenna boresight is in the $+z$ direction. . . . .	35
23	“H-plane” pattern of the two foot dish at 10 GHz. Effect of tilting the AUT in the Azimuth plane versus the Elevation plane. Notice that the Azimuth pattern at a constant Elevation offset (dashed curve) is a conical cut and not a principal plane cut. . . . .	35
24	“E-plane” pattern of the two foot dish at 10 GHz. Effect of tilting the AUT in the Azimuth plane versus the Elevation plane. . . . .	36
25	Dish-plus-splash-plate antenna system geometry. The splash plate is rectangular with dimensions of 36 by 26.4 inches. . . . .	37
26	Configuration A for the dish and splash plate. . . . .	38
27	Configuration B for the dish and splash plate. . . . .	39
28	Comparison of the H-plane far-zone pattern at 10 GHz obtained using Configuration B in Figure 27 versus Configuration A in Figure 26. The orientation of the dish is $\tau = 90$ degrees. . . . .	39
29	Comparison of the E-plane far-zone pattern at 10 GHz obtained using Configuration B in Figure 27 versus Configuration A in Figure 26. The orientation of the dish is $\tau = 90$ degrees. . . . .	40
30	Comparison of the E-plane far-zone pattern at 10 GHz obtained using Configuration B in Figure 27 versus Configuration A in Figure 26. The orientation of the dish is $\tau = 0$ degrees. . . . .	40
31	Comparison of the H-plane far-zone pattern at 10 GHz obtained using Configuration B in Figure 27 versus Configuration A in Figure 26. The orientation of the dish is $\tau = 0$ degrees. . . . .	41
32	The near-field distribution of the dish-plus-splash-plate antenna system as measured in Configuration A at 10 GHz. This distribution is truncated at $x = -20$ and $x = -12$ to examine the usefulness of the new GO based rule of thumb. . . . .	43
33	Effect of truncating the near-field data at various $x$ locations. The GO based rule of thumb predicts the pattern to be valid for $AZ > -6$ degrees and $AZ > -11$ degrees when the near-field data is truncated at $x = -12$ inches and $x = -20$ inches, respectively. . . . .	44

34	Configuration to measure the dish alone and obtain the electromagnetic fields incident on the splash plate in the dish-plus-splash-plate system. The size of the splash plate is shown as a heavy line in the scan plane. The subtended angles (4 and 10 degrees) in the Azimuth plane for the splash plate are also shown. The subtended angles in the Elevation plane are 31.3 degrees for the full data set and 1.7 degrees for the truncated data set. . . . .	45
35	Measured incident field distribution on the splash plate as shown in Figure 34. The frequency is 10 GHz and the polarization is $\hat{y}$ ( $\tau = 90$ ). . . . .	46
36	Effect of truncating the near-field data to the size of the splash plate as shown in Figure 35. The near-field range configuration is shown in Figure 34 and the polarization is $\tau = 90$ . . . . .	47
37	Effect of truncating the near-field data to the size of the splash plate as shown in Figure 35. The near-field range configuration is shown in Figure 34 and the polarization is $\tau = 90$ . . . . .	47
38	Effect of truncating the near-field data to the size of the splash plate. The near-field range configuration is shown in Figure 34 and the polarization is $\tau = 0$ . . . . .	48
39	Effect of truncating the near-field data to the size of the splash plate. The near-field range configuration is shown in Figure 34 and the polarization is $\tau = 0$ . . . . .	48
40	The splash plate is simulated by truncating the measured near-field of the dish alone. The far-zone pattern from this simple simulation is compared with the pattern obtained from measuring the dish-plus-splash-plate system. Measured results using Configuration A (Figure 26) and Configuration B (Figure 27) are shown. The polarization is $\tau = 90$ . . . . .	49
41	The splash plate is simulated by truncating the measured near-field of the dish alone. The far-zone pattern from this simple simulation is compared with the pattern obtained from measuring the dish-plus-splash-plate system. Measured results using Configuration A (Figure 26) and Configuration B (Figure 27) are shown. The polarization is $\tau = 90$ . . . . .	49
42	The splash plate is simulated by truncating the measured near-field of the dish alone. The far-zone pattern from this simple simulation is compared with the pattern obtained from measuring the dish-plus-splash-plate system. Measured results using Configuration A (Figure 26) and Configuration B (Figure 27) are shown. The polarization is $\tau = 0$ . . . . .	50



43	The splash plate is simulated by truncating the measured near-field of the dish alone. The far-zone pattern from this simple simulation is compared with the pattern obtained from measuring the dish-plus-splash-plate system. Measured results using Configuration A (Figure 26) and Configuration B (Figure 27) are shown. The polarization is $\tau = 0$ . . .	50
44	Sketch of the various splash plate deformations. The concave plate is concave when one is looking at the splash plate from the dish's point of view and similarly for the convex plate. . . . .	51
45	Azimuth pattern of dish-plus-splash-plate antenna with a flat and a concave splash plate. Configuration A in Figure 26 was used and the dish is polarized horizontally or "in the plane of the paper" ( $\tau = 0$ ). .	52
46	Azimuth pattern of dish-plus-splash-plate antenna with a flat and a convex splash plate. Configuration A in Figure 26 was used and the dish is polarized horizontally or "in the plane of the paper" ( $\tau = 0$ ). .	53
47	Azimuth pattern of dish-plus-splash-plate antenna with a flat and a odd splash plate. Configuration A in Figure 26 was used and the dish is polarized horizontally or "in the plane of the paper" ( $\tau = 0$ ). . . . .	53

## List of Tables

1	Planar near-field measurement error sources [1] . . . . .	14
2	Some useful self comparison tests. . . . .	16
3	The relative magnitude of the erroneous grating lobe for various values of probe position error, $\epsilon$ , when $\Delta = 0.5$ inches and $\lambda = 1.18$ inches. .	34
4	The relative position of the erroneous grating lobe for various frequencies when $\theta_0 = -45$ degrees and $\Delta = 0.5$ inches. . . . .	34
5	The GO based rule of thumb applied to the measurement in Figures 32 and 33. . . . .	44
6	Squint errors caused by deformation of the splash plate in the dish-plus-splash-plate antenna system. The measurements referred to here were performed using Configuration A in Figure 26. . . . .	52

# 1 INTRODUCTION

Planar near-field antenna measurements are increasing in popularity for several reasons [2]. Near-field measurements are easily performed indoors in a relatively small and environmentally stable facility as compared with outdoor far-zone measurements. In addition, the test antenna is stationary in a planar near-field measurement which is important for large cumbersome antenna systems or delicate space antennas. In addition, near-field facilities may be located very close to spacecraft assembly areas to minimize the risk of moving flight hardware to a separate measurement location.

This investigation is motivated by the difficulty of measuring certain multiple reflector antenna systems in a typical near-field range configuration. The three primary objectives of this investigation are: (1) to investigate alternative planar near-field measurement configurations, (2) to support computational simulation studies [3] (not discussed here) by providing a measurement baseline and some measure of measurement accuracy and (3) to investigate the performance of a particular dish-plus-splash-plate antenna system.

In a typical planar near-field antenna measurement, the test antenna is pointed such that its boresight is perpendicular to the scan plane. This conventional arrangement minimizes some sources of error, such as probe characterization error, and simplifies the coordinate system issues since the scanner coordinate system is aligned with the test antenna. Unfortunately, some complex antenna systems are not easily arranged such that the boresight is perpendicular to the scan plane. The conventional arrangement also places a practical limit to the maximum far-zone angles (as measured from the boresight direction) that can be measured. An alternative near-field measurement configuration has the boresight of the test antenna at an oblique angle with respect to the scan plane. This alternative configuration is called a "tilted antenna" arrangement. When the antenna is tilted, some of the usual near-field measurement errors are increased. The most important and most difficult errors to compensate for are those associated with the probe. In a tilted antenna configuration, it is important to have a well characterized probe where the far-zone patterns of the probe are known for large angles. Another issue to be dealt with is the appropriate size and position of the scan area when the antenna is tilted. A new simple rule of thumb based on geometrical optics is provided that relates the scan area size and position to the maximum desired far-zone angles. Since this new rule of thumb is based on geometrical optics, it is very easy to apply to multiple reflector antenna systems. Also, this rule of thumb is expected to be most accurate for small angles as measured from the boresight direction. The tilted antenna configuration allows one to measure the sidelobes far from the boresight direction, which is demonstrated by some measurement results for angles as far as 120 degrees. In general, it is concluded that a tilted antenna configuration with a tilt angle as large as 45 degrees will provide measurements that are accurate enough for many applications.

One method of evaluating the quality of a near-field range is to test the same antenna in different measurement configurations which ideally should provide identical results. These types of comparisons are called “self comparison” tests. An example is comparing the results from a normal antenna configuration to results from a tilted antenna configuration. Another method is to compare results from the near-field range to an independent result from another measurement range. By performing various self comparison tests and comparing the results from the near-field range to results from another range, a measure of the repeatability and accuracy for testing a particular type of antenna can be established. The measure of accuracy of the near-field range will obviously depend on the assumed accuracy of the other independent range. Nonetheless, these types of comparisons can be very useful for establishing real world confidence levels. These approximate accuracy levels can be quite useful when comparing the measured results with computer simulations.

In addition to the investigation of the measurement issues described above, a particular dish-plus-splash-plate antenna system is evaluated. Several deterministic deformations of the splash plate are of interest and the effect of these deformations on the far-zone patterns of the antenna system are presented. It is shown that the far-zone main beam of the antenna system is squinted when the splash plate is deformed and that the measured magnitude of this squint agrees well with the predicted squint from a simple analysis.

An  $e^{j\omega t}$  time convention is assumed and suppressed throughout this paper.

## 2 PLANAR NEAR-FIELD ANTENNA MEASUREMENTS

### 2.1 Antenna Measurement Methods

There are many different antenna measurement methods for obtaining the radiation characteristics of a test antenna, but the three most commonly used methods are the far-zone range, the compact range and the near-field range. Each of these methods has numerous variations; for example the far-zone range may be implemented outdoors or inside an anechoic chamber depending on the particular requirements.

In a far-zone range, the test antenna is mounted on a positioner and communicates with another antenna which is far away. In particular, the two antennas are usually separated by  $R$  where

$$R > \frac{2D^2}{\lambda}$$

and  $D$  is a defining size parameter for the antenna under test (AUT) (such as the diameter for a circular reflector antenna) and  $\lambda$  is the wavelength. As  $D$  becomes larger or  $\lambda$  becomes smaller, the separation distance  $R$  becomes much larger. This explains why many far-zone measurements are performed outdoors, since the separation distance may be on the order of thousands of feet for some test antennas.

A compact range uses a large parabolic reflector antenna to illuminate a test antenna which is mounted on a positioner. The test antenna is placed in the near-field of the large reflector which is usually quite larger than the test antenna. Because of the nature of the parabolic reflector, the test antenna is effectively illuminated by a collimated plane wave and in this manner, the compact range simulates a far-zone range but requires much less space. In fact, a compact range is typically inside an anechoic chamber. Note that in practice the test antenna may illuminate the reflector instead of the reflector antenna illuminating the test antenna.

A near-field range differs from a far-zone range and a compact range in that the far-zone characteristics of the test antenna are not directly measured in real time. In a near-field range, the radiating fields from the test antenna are probed in the near-zone of the test antenna, typically around 5 to 20 wavelengths away, and then this near-zone data is processed in a computer to finally obtain the far-zone characteristics of the test antenna. In this manner, a near-field antenna measurement is an indirect measurement. The near-zone fields may be measured by scanning the probe on any convenient coordinate surface, such as a sphere, a cylinder or a plane. The most popular scan surface is a plane. In practice, the test antenna may be the receiver while the probe is the transmitter.

## 2.2 Motivation for Planar Near-field Antenna Measurements

One is motivated to use a planar near-field range for many reasons. To begin with, a planar near-field range requires much less space than a far-zone range since the test antenna fields are probed relatively close to the test antenna. This allows the near-field measurement to be performed indoors in a more secure and environmentally stable space. In addition, for antennas with high directivity, one can perform near-field measurements in a room which is not a complete anechoic chamber. Another advantage of planar near-field measurements is that the test antenna is mounted in a stationary position while the probe moves along a planar surface near the test antenna. This can be a significant advantage if the test antenna is delicate or mounted on a structure which is not easily placed on a rotating positioner.

## 2.3 Basic Concepts of a Planar Near-field Antenna Measurement

A planar near-field measurement includes the following steps: (1) the electromagnetic field close to the AUT is measured by scanning a probe over a planar surface in front of the AUT, (2) the data is collected and processed in a computer to obtain the far-zone characteristics of the AUT. There are several important parameters in the near-field range which affect the accuracy and usefulness of the measurement, such as the size of the scan plane, the sample spacing and probe position accuracy.

The size of the scan plane is ideally an infinite planar surface but realistic facilities are finite. Therefore, one must determine how large the finite scan plane must be for the particular AUT and accuracy requirements. The necessary size of the scan plane is determined primarily by two concerns. The first concern is the largest far-zone angle of interest as measured from the boresight of the AUT and the second is the relative amplitude of the fields at the edges of the scan plane. When measuring simple antennas with well defined apertures, the commonly used rule of thumb that defines the maximum far-zone angle, as shown in Figure 1, is

$$\theta_m = \arctan\left(\frac{L - D}{2d}\right) \quad (1)$$

where  $\theta_m$  is the maximum far-zone angle of interest,  $L$  is the size of the scan plane,  $D$  is the size of the AUT aperture and  $d$  is the separation distance between the AUT and the scan plane [1, 8]. Equation 1 is valid for the two-dimensional case but can be easily generalized for three dimensions. Equation 1 can be used to determine what size scan plane is necessary to obtain the far-zone pattern of the test antenna out to an angle  $\theta_m$ . This rule of thumb works well for simple antennas which have an easily defined aperture, but a new more general rule of thumb will be presented later in Section 3.1.3. To determine how small the relative level of the fields at the edge

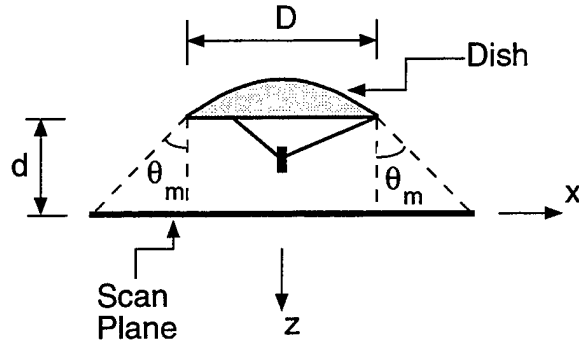


Figure 1: Rule of thumb defining the maximum far-zone angle  $\theta_m$  as a function of the AUT aperture size  $D$ , scan plane size  $L$  and the scan to AUT separation distance  $d$ .

of the scan plane must be for any given level of measurement uncertainty, one can use the error analysis published by Newell or Yaghjian [8, 1]. On the other hand, a useful starting point is a simple rule of thumb given by Slater [4] which states that the fields at the edges of the scan plane should be smaller than the lowest relative sidelobe level of interest.

The sample spacing must be chosen small enough to minimize aliasing errors. The far-zone pattern of the AUT is directly related to the Fourier transform of the near-field scan data which is sampled on a periodic grid. It is well known from the spatial Nyquist criterion that the sample spacing should be less than half a wavelength of the highest frequency in the spectrum assuming that the spectrum is bandlimited. Normally, the evanescent (not propagating) portion of the Fourier spectrum is very small compared to the radiating portion and therefore the spectrum is effectively bandlimited. However, this assumption may not be valid for some particular types of antennas where the multiple interaction between the probe and antenna is significant [10, 11, 12]. Using this assumption and the spatial Nyquist sampling criterion one finds that the sample spacing  $\Delta$  should satisfy

$$\Delta < \frac{\lambda}{2} \quad (2)$$

where  $\lambda$  is the wavelength. This requirement can be loosened somewhat if the test antenna has a very narrow beam such that the spectrum of the measured data is expected to be very small after some angle  $\theta_0$ . For these types of narrow beam antennas one may use

$$\Delta < \frac{\lambda}{2 \sin \theta_0} \quad (3)$$

The necessary probe position accuracy is dependent on the frequency and the required accuracy of the measurement. Although one can use the general formulas for upper bound error estimates in [1, 8], it is useful to first use a more general

simple requirement. To measure gain with accuracy on the order of 0.1 dB and 30 dB sidelobes on the order 0.2 dB, the probe position accuracy must be [13, 14]

$$\delta < \frac{\lambda}{50} \quad (4)$$

where  $\delta$  is the maximum deviation from a perfect planar rectangular grid.

Another important parameter which must be determined when setting up a planar near-field measurement is how far to place the AUT from the scan plane. In general, one can place the scan plane anywhere in the radiating near-field region in front of the AUT where the radiating near-field region extends from about one wavelength to a distance of  $2D^2/\lambda$ . In order to obtain accurate far-zone patterns out to a reasonable angle  $\theta_m$ , one should place the scan plane as close as possible to the AUT, but this may increase the multiple interactions between the probe/scanner and the AUT. Recall that the near-field data processing assumes that there is only a first order coupling between the probe and the AUT and therefore all multiple interactions between the probe/scanner and the AUT cause errors in the final results. The best choice of the separation distance must take into account the desire to maximum the distance (to minimize the AUT and probe/scanner interaction) and the desire to minimize the distance (to maximize the measurable far-zone angle). Therefore this separation distance must be chosen on a case by case basis depending the application where a typical distance is anywhere from 5 to 30 wavelengths.

### 2.3.1 Near-field to Far-zone Transformation

There is a simple Fourier relationship between the field located on a planar surface in front of the AUT and the field in the far-zone of the AUT [15, 16]. In particular, consider the Fourier transform of the field located in the  $z = 0$  plane in front of the radiating AUT,

$$\mathbf{F}(\mathbf{k}) = \frac{1}{4\pi^2} \int_{-\infty}^{\infty} \int_{-\infty}^{\infty} \mathbf{E}^a(x, y, 0) e^{jxk_x} e^{jyk_y} dx dy \quad (5)$$

where  $\mathbf{E}^a(x, y, 0)$  is the AUT electric field located on the  $z = 0$  plane and the wave vector is  $\mathbf{k} = k_x \hat{\mathbf{x}} + k_y \hat{\mathbf{y}} + k_z \hat{\mathbf{z}}$ . In terms of the spherical coordinate angles  $(\theta, \phi)$  or the Azimuth-Elevation angles  $(A, E)$ ,

$$\begin{aligned} k_x &= k \sin \theta \cos \phi = k \sin A \cos E \\ k_y &= k \sin \theta \sin \phi = k \sin E \\ k_z &= k \cos \theta = k \cos A \cos E \end{aligned}$$

where  $k = 2\pi/\lambda$ . Note that the Azimuth angle,  $A$ , used here follows the convention used at NIST which is different by a minus sign from the convention used by Scientific-Atlanta [17, 18, 5]. Now, the radiated far-zone field (at  $|\mathbf{r}| \rightarrow \infty$ ) of the AUT is

$$\mathbf{E}(\mathbf{r}) = j2\pi k_z \mathbf{F}(\mathbf{k}_0) \frac{e^{-jk r}}{r} \quad (6)$$

where  $\mathbf{k}_0 = k\hat{\mathbf{r}}$ . As seen from Equations 5 and 6, all one needs to do is measure the electric field on a planar surface in front of the AUT and perform a Fourier transform of this field to obtain the far-zone patterns of the AUT. Unfortunately, it is not possible to measure the near-field of the AUT unless one has an ideal probe. To perform accurate near-field measurements, the directivity of the probe must be taken into account. This can be done by performing what is called probe compensation.

### 2.3.2 Probe Compensation

Probe compensation in an antenna near-field measurement refers to the process of removing the first order effect of the non-ideal probe from the measurement results. Using reciprocity, the following formula can be derived [16]

$$\mathbf{E}^a(k_x, k_y) \cdot \mathbf{E}^b(-k_x, k_y) = k_z C \int_{-\infty}^{\infty} \int_{-\infty}^{\infty} P(x', y') e^{j\mathbf{k} \cdot \mathbf{r}'} dx' dy' \quad (7)$$

where  $C$  is a constant,  $\mathbf{E}^a(k_x, k_y)$  is the far-zone radiated electric field of the AUT,  $\mathbf{E}^b(k_x, k_y)$  is the far-zone radiated electric field of the probe and  $P(x', y')$  is the measured probe response as a function of the probe position  $(x', y')$ . An alternative and equivalent formulation based on scattering matrix theory can also be used [1, 7]. Equation 7 demonstrates that the far-zone pattern of the probe,  $\mathbf{E}^b(k_x, k_y)$ , must be known to the same level accuracy at which the AUT pattern,  $\mathbf{E}^a(k_x, k_y)$ , is desired. Also, because of the vector nature of the far-zone fields another equation like Equation 7 is necessary to solve for the unknown AUT far-zone field. This second equation can be obtained by using a second probe. If the first probe is linearly polarized, then the second required equation can be obtained by simply rotating the probe 90 degrees about its boresight axis and used again.

### 2.3.3 Sources of Error

There are many possible sources of error in a near-field antenna measurement just as there are in any type of antenna measurement. Over the years, there has been some effort to quantify the significant errors in a planar near-field measurement [19, 1, 13]. Table 1 is a list of errors compiled and studied by NIST (previously called NBS) which is often used [1]. The errors in Table 1 can be quantified by computer simulations, measurement tests or theoretical formulas.

## 2.4 Near-field Range Validation and Diagnostics

Near-field range validation starts with the quantification of the various error sources, such as those listed in Table 1, and establishing an error budget [1, 13]. With the



Table 1: Planar near-field measurement error sources [1]

1)	Probe pattern
2)	Probe polarization ratio
3)	Probe gain
4)	Probe alignment error
5)	Normalization constant
6)	Impedance mismatch factor
7)	AUT alignment error
8)	Data point spacing
9)	Measurement area truncation
10)	Probe translational position errors ("x" and "y" errors)
11)	Probe normal position errors ("z" errors)
12)	Multiple interaction between AUT and probe/scanner
13)	Receiver amplitude nonlinearity
14)	System phase error (Receiver, cables, rotary joints, etc.)
15)	Receiver dynamic range
16)	Room Scattering
17)	Leakage and crosstalk
18)	Random errors in amplitude/phase

error budget, one can compute error bounds for the measured AUT parameters such as gain and sidelobe level. Nonetheless, it may still be necessary to perform further tests to insure that the error budget is accurate and to verify that there are no other significant errors which have not already been accounted for. Also, some errors may be more or less significant depending upon the particular test antenna.

The common measurement tests used for near-field range validation can be grouped into three categories:

1. Comparison with other independent measurements such as far-zone or compact range measurements.
2. Comparison with computer simulations.
3. Self comparison tests.

The first two categories listed above involve comparisons with other methods of evaluation which also contain errors. Although these types of comparisons can be very useful, it is often difficult to determine if the errors are associated with the near-field measurement or with the other method of evaluation. Even when the error can be attributed to the near-field measurement, these first two types of comparison normally don't provide any diagnostic information. On the other hand, the third category "Self comparison tests" can help to quantify error sources in the near-field measurement and provide some diagnostic information. Self comparison tests involve measuring the AUT in the near-field range multiple times in slightly different configurations where an ideal measurement range would provide identical results. For example, the AUT is measured once and then moved to a slightly different location and measured again. If the AUT movement between measurements is in a direction normal to the scan plane ("z" direction) then this self comparison test will provide information about the errors caused by the multiple interaction between the probe/scanner and the AUT. Table 2 lists some useful self comparison tests and the error sources which are relevant to the tests.

There are other methods which can be used for range diagnostics besides the antenna measurements described above. Some of the self comparison tests can be performed by data processing rather than actually performing multiple measurements. For example, the effect of various scan plane sizes can be investigated by simply truncating the near-field data in the computer. Also the sample spacing can be investigated by performing an antenna measurement with a relatively small sample spacing and then processing the data at different levels of decimation to investigate other sample spacings that are integer multiples of the original sample spacing. In addition to these simplistic data processing investigations, one can also use microwave holography or radar imaging techniques [4].

Table 2: Some useful self comparison tests.

Test Description	Relevant Error Source
AUT orientation	AUT and probe/scanner interactions which cause polarization errors
AUT placement relative to scanner	AUT and probe/scanner interactions
Absorber placement	Room Scattering
Scan plane size	Scan plane truncation
Sample spacing	Aliasing errors
Repeatability tests	Random errors

If the range instrumentation has the ability to perform swept frequency measurements then the data can be transformed into the time domain to obtain useful information about multiple interactions and room scattering error sources. In some ranges, it may be possible to directly measure the time domain probe response and even use time domain gating during a near-field measurement.

### 3 TILTED ANTENNA CONFIGURATIONS

The most common approach when setting up a planar near-field antenna measurement is to point the AUT normal to the scan plane or in other words the AUT boresight is perpendicular to the scan plane. This type of arrangement minimizes the probe characterization errors and simplifies the coordinate system issues since the AUT coordinate system and the scanner coordinate system are different only in a simple "z" translation. Nonetheless, sometimes it is not practical to use this conventional type of arrangement. For example, certain complex multiple reflector antenna systems are not easily arranged such that the main beam is normal to the scan plane. Also, there is a theoretical limitation of 90 degrees for the maximum far-zone angle (as measured off boresight) that can be obtained from the conventional configuration and in most practical situations this limitation is 60 or 70 degrees.

This section describes an investigation of alternative near-field range configurations where the antenna is tilted at an oblique angle with respect to the scan plane. Not only is this more convenient for certain multiple reflector antenna systems but also the far-zone patterns can be obtained at much larger angles as measured off the antenna boresight. First, the significant measurement errors which are particularly important when the antenna is tilted with respect to the scan plane are discussed then a series of numerical examples are presented.

#### 3.1 Significant Sources of Error for a Tilted Antenna Configuration

When the test antenna is tilted with respect to the scan plane there are particular error sources which may be more significant. From Table 1, the following errors would obviously be of more concern

- 1) Probe pattern
- 2) Probe polarization ratio
- 8) Data point spacing
- 9) Measurement area truncation
- 10) Probe translational position errors  
("x" and "y" errors)
- 12) Multiple interaction between  
AUT and probe/scanner
- 16) Room Scattering

Most of these errors can be minimized in the usual way. For example, the room scattering can be minimized by proper absorber placement. The most difficult errors

to minimize are those associated with the probe; such as probe pattern errors or probe and AUT multiple interactions. In addition to the error sources listed above or in Table 1 there are also other issues which must be dealt with when the AUT is tilted, such as coordinate system and polarization conventions.

### 3.1.1 Probe Characterization Errors

Errors in the knowledge of the probe far-zone relative patterns directly translate into errors in the AUT far-zone patterns because the probe patterns change the AUT far-zone patterns decibel for decibel when the probe compensation is computed. This means that if the relative probe pattern is wrong by 0.5 dB at a particular direction then the resulting far-zone pattern of the AUT will be wrong by 0.5 dB in the corresponding direction. Normally, a very broadbeam probe is used such as an open ended waveguide (OEWG) and only the probe pattern near boresight is needed when the AUT is pointed normal to the scan plane. On the other hand, when the AUT is tilted at an oblique angle with respect to the scan plane, say 45 degrees for example, then the probe pattern out at 45 degrees off boresight is used in the probe compensation for the AUT main beam. This requires that one know the probe pattern accurately at 45 degrees off boresight in order to obtain accurate patterns from the tilted AUT arrangement. Not only can this affect the sidelobe levels of the AUT but it can also affect the measured peak gain of the AUT. The best way to avoid this error is to obtain a very accurate probe characterization even for large far-zone angles. Also, the probe patterns are normally best characterized in the principal planes so it is wise to tilt the AUT in the “xz” or “yz” plane relative to the scanner.

### 3.1.2 Insufficient Sampling

The near-field data point spacing must be chosen appropriately when the AUT is tilted with respect to the scan plane. If a sample spacing of  $0.5\lambda$  or smaller is chosen to avoid aliasing errors then this should still work when the AUT is tilted. However, when the AUT has a very narrow beamwidth the sample spacing can normally be chosen larger without introducing any significant error. If all of the significant radiated power from the AUT is contained within a far-zone angle of  $\theta_m$  then the sample spacing  $\Delta$  may be chosen as

$$\Delta < \frac{\lambda}{2 \sin \theta_m} \quad (8)$$

for an AUT pointed normal to the scan plane. But when the the AUT is tilted at an angle  $\theta_T$  with respect to the scan plane normal then the sample spacing should be

$$\Delta < \frac{\lambda}{2 \sin (\theta_m + \theta_T)} \quad (9)$$

where this equation is valid for  $(\theta_m + \theta_T) < 90$  degrees. For example, if all of the significant radiated power from the AUT is contained within an angle of  $\theta_m = 25$  degrees then, from Equation 8, the maximum sample spacing is  $\Delta = 1.2$  wavelengths; but if the AUT is tilted at an angle of  $\theta_T = 45$  degrees then, from Equation 9, the maximum sample spacing is 0.53 wavelengths.

### 3.1.3 Scan Area Truncation

Theoretically, the size of the scan area in a planar near-field measurement should be an infinite plane but unfortunately infinite planes are difficult to use in a real measurement facility. So, there is always some error caused by the finite size of the scan plane and one must choose the proper size of the scan area depending on the test antenna and the required far-zone patterns. As described earlier (see Figure 3 and Equation 1), there is a commonly used rule of thumb to help one choose the size of the scan plane, but this rule of thumb is not applicable for a multiple reflector antenna system with a beam tilted with respect to the scan plane. For this more general case, a useful rule of thumb based on geometrical optics, instead of diffraction, which relates the scan size to the maximum far-zone angle of interest is as follows

1. Trace the geometrical optics (GO) rays through the antenna system and observe where they land on the scan plane.
2. Notice that the GO rays form a collimated beam in the near-field of the AUT.
3. Measure the maximum allowable far-zone angles from the GO collimated beam to the edges of the scan plane.

See Figures 10, 13, 26, 27 and 34 for examples of the above rule of thumb.

### 3.1.4 Translational Probe Position Errors

The necessary probe position accuracy is dependent on the frequency of operation as expressed in the rule of thumb in Equation 4. However, this equation does not differentiate probe position errors in the normal or "z" direction versus errors in the translational directions ("x" or "y"). For the typical arrangement where the AUT is pointed normal to the scan plane, the measurement accuracy is more sensitive to probe position errors in the normal ("z") direction because these position errors correspond directly to phase errors in the near-field data. On the other hand, for a tilted antenna configuration, probe position errors in the normal and translational

directions correspond to phase errors in the near-field data and therefore one must ensure that the probe position is known very accurately in both the normal and translational directions.

### **3.1.5 Room Scattering**

As in any indoor antenna measurement, unwanted electromagnetic scattering from objects (such as walls, floors and equipment) in the room can cause errors in the measurement. When measuring a highly directive antenna in a near-field range it is very important to place absorber wherever the collimated beam from the AUT is pointed. In the typical arrangement where the AUT is pointed normal to the scan plane, this corresponds to placing absorber on and behind the scanner. For a tilted antenna arrangement, similar absorber placement with some small modifications is usually adequate.

### **3.1.6 Coordinate System Convention Issues**

When the antenna is tilted with respect to the scan plane, one needs to pay special attention to the coordinate system and polarization conventions that are used to express the far-zone patterns computed from the near-field data. Normally, the far-zone patterns are expressed in a coordinate system fixed on the scan plane since this is the most natural and consistent one to use. In the typical arrangement there is only a simple offset in the "z" direction (normal direction) between the AUT coordinate system and the scanner coordinate system which only causes a difference in the phase of the far-zone fields. Unfortunately, for the tilted AUT arrangement, the coordinate system of the AUT is tilted and offset from the scanner coordinate system which can cause some confusion if not handled properly. In all of the numerical results in this paper, the AUT is tilted in the "x-z" plane which corresponds to the Azimuth plane. When this is done there is simply an Azimuth offset between the far-zone coordinate system fixed on the scanner and the one fixed on the AUT. If the offset was in the Elevation plane then the Azimuth patterns plotted at the constant Elevation offset angle would be conical cuts instead of the desired principal plane great circle cuts. This can be visualized using Figure 22.

## **3.2 Measurement Results of the Two Foot Dish**

This section presents various measurement results of the two foot diameter dish which demonstrate the concepts discussed earlier. All of the measurements are performed at X-band (8-12 GHz).

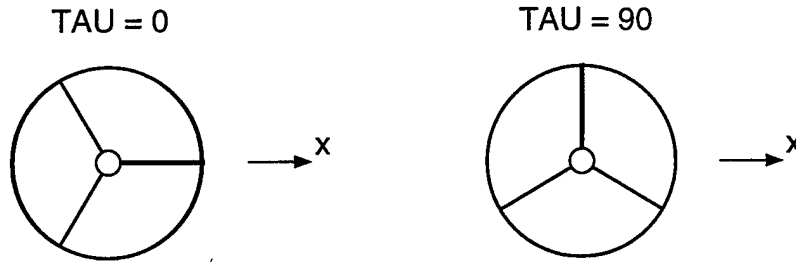


Figure 2: Definition of  $\tau$  (“TAU”) angle. For  $\tau = 0$  the electric field is polarized in the  $x$  direction and for  $\tau = 90$  the electric field is polarized in the  $y$  direction.

The Aerospace Corporation’s planar near-field range is in a semi-anechoic chamber which has absorber covering two walls and the ceiling. Numerous additional absorber panels (approximately 6 by 4 feet in size) are positioned throughout the range as needed for any particular AUT. The scan area has a maximum size of approximately 9 (horizontal) by 6 (vertical) feet. The scanner control and data collection is implemented by a controller box and software from Near-field Systems Incorporated (NSI) but additional data processing can also be done using the MATLAB computer program. The microwave source and receiver are implemented by using an HP 8510B network analyzer. The probe is an X-band WR90 open ended waveguide with a 6 dB waveguide attenuator. The probe compensation uses an approximate closed form characterization derived by Yaghjian [20].

The measurements of a two foot diameter center fed parabolic reflector are presented. The reflector (TRG model 822024B-188/383) has a focal length of 8 inches. The feed, which is held up by three aluminum spars of diameter 0.5 inches, is an open ended circular waveguide. The feed inner diameter is 0.9 inches and outer diameter is 1.4 inches. The coax to waveguide transition on the feed is a Maury model X230A1.

Figure 2 shows the polarization orientation of the dish with respect to the scanner coordinate system ( $x, y, z$ ) as a function of the angle  $\tau$  (“TAU”). This figure also shows the symmetrical three spars which hold the feed antenna. The various  $\tau$  positions are well defined by the coax cable which runs along one of the spars to the feed antenna. In the  $\tau = 0$  position, the coax cable runs along the horizontal spar (parallel to  $\hat{x}$ ). In the  $\tau = 90$  position the coax cable runs along the vertical spar (parallel to  $\hat{y}$ ). The dish linearly polarized in a direction parallel to  $\hat{x}$  or  $\hat{y}$  when  $\tau = 0$  or  $\tau = 90$ , respectively.

### Example: Comparison with Far-zone Range Measurements

The far-zone range located on the roof of A2 was used as an independent measurement facility for comparison with the results from the near-field range. The far-zone range length was approximately 80 feet.



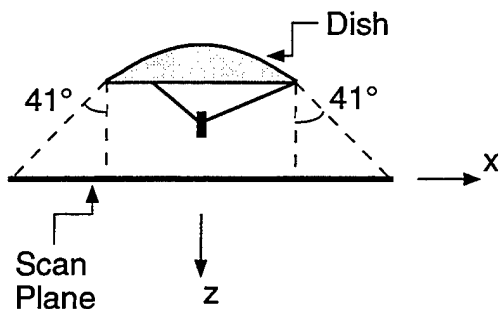


Figure 3: The dish is pointed in the same direction as the normal vector of the scan plane. This is the conventional configuration.

The TRG dish was measured in the near-field range as shown in Figure 3. Figures 4 through 9 show the principal plane patterns of the TRG dish as measured in the near-field range versus the far-zone range. There are two dashed curves in each of these figures corresponding to two far-zone range measurements where the second measurement is obtained with the dish rotated 180 degrees about its axis. This second pattern is flipped and if the far-zone range was perfect the two dashed curves would be identical. For the 10 GHz case, shown in Figures 6 and 7, the dish was measured in the near-field range with  $\tau = 0$  and  $\tau = 90$  as shown in Figure 2. These two measurements are plotted together, as shown by the two solid curves in Figures 6 and 7, by making appropriate changes in the coordinate system. The two solid curves would be identical if the near-field measurements were perfect.

#### Example: Comparison between “tilted” and normal configurations.

The dish was measured in the near-field range in the normal configuration shown in Figure 3 and also a tilted configuration shown in Figure 10. The dish is pointed at an angle of 45 degrees with respect to scan plane in the tilted configuration. The size and position of the scan area is adjusted to obtain far-zone pattern information as far as approximately 25 degrees off boresight as predicted by the GO based rule of thumb discussed earlier in Section 3.1.3.

Figures 11 and 12 show the E-plane and H-plane principal plane patterns of the two foot dish. There are six curves in each plot; two curves correspond to the conventional near-field range configuration shown in Figure 3 and four curves correspond to the tilted configuration shown in Figure 10. The multiple curves correspond to measurements of the dish at various  $\tau$  positions where the  $\tau = 0$  and  $\tau = 90$  degree cases are defined in Figure 2.

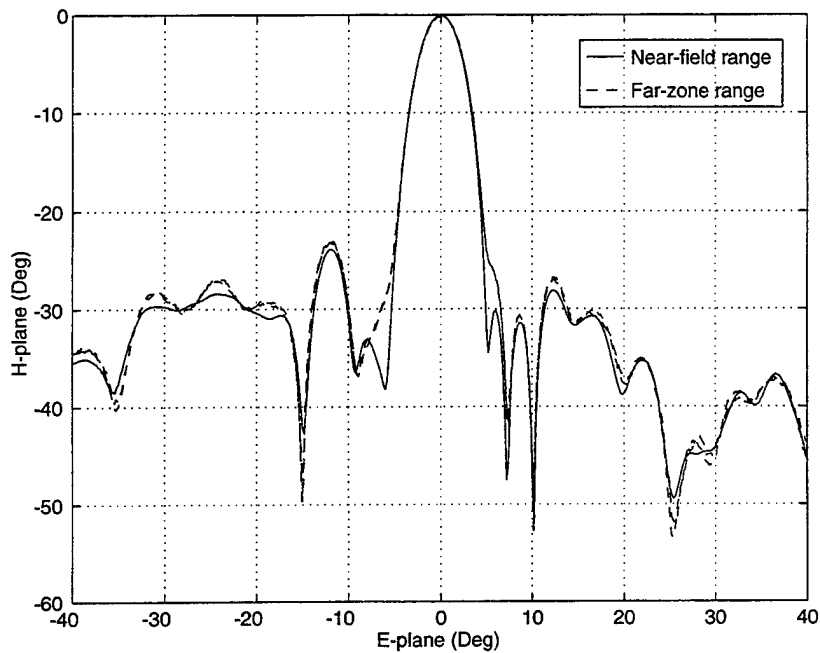


Figure 4: Comparison of E-plane far-zone pattern obtained from the far-zone range versus the near-field range at 9 GHz. The orientation of the dish in the near-field range is shown in Figure 3.

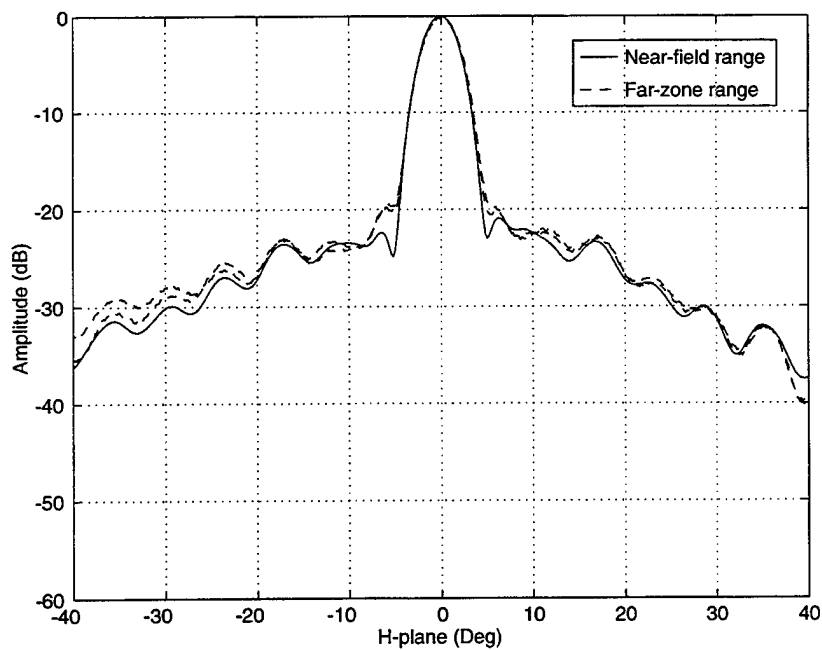


Figure 5: Comparison of H-plane far-zone pattern obtained from the far-zone range versus the near-field range at 9 GHz. The orientation of the dish in the near-field range is shown in Figure 3.

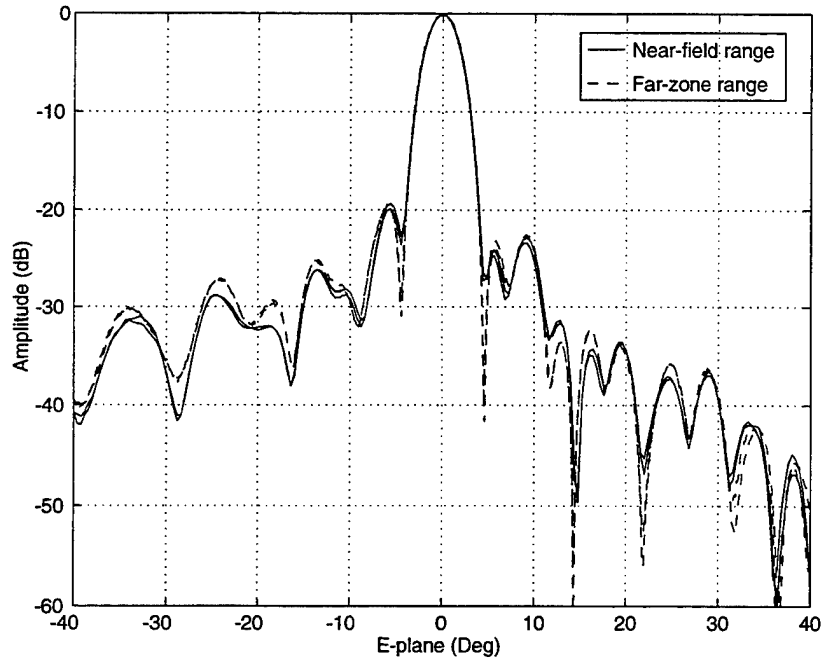


Figure 6: Comparison of E-plane far-zone pattern obtained from the far-zone range versus the near-field range at 10 GHz. The orientation of the dish in the near-field range is shown in Figure 3.

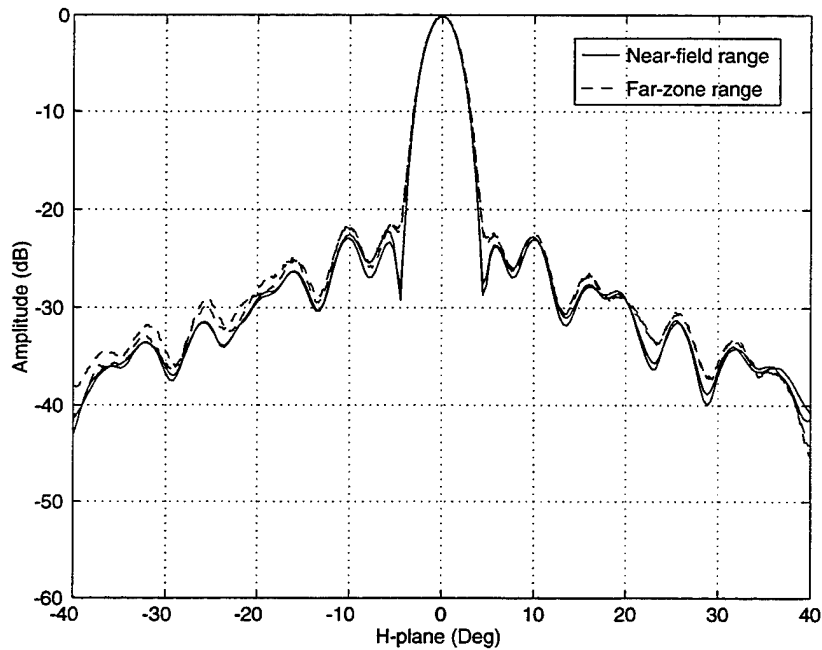


Figure 7: Comparison of H-plane far-zone pattern obtained from the far-zone range versus the near-field range at 10 GHz. The orientation of the dish in the near-field range is shown in Figure 3.

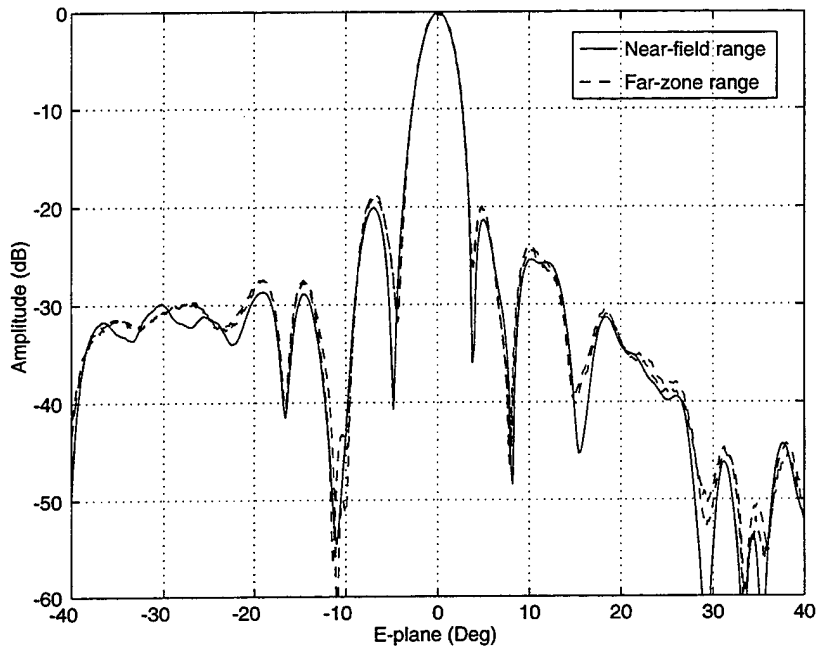


Figure 8: Comparison of E-plane far-zone pattern obtained from the far-zone range versus the near-field range at 11 GHz. The orientation of the dish in the near-field range is shown in Figure 3.

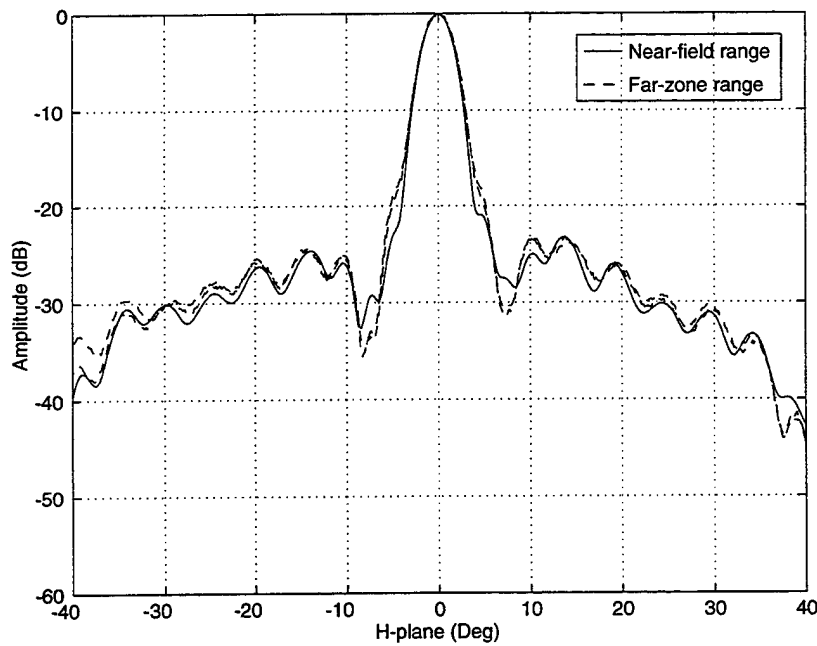


Figure 9: Comparison of H-plane far-zone pattern obtained from the far-zone range versus the near-field range at 11 GHz. The orientation of the dish in the near-field range is shown in Figure 3.

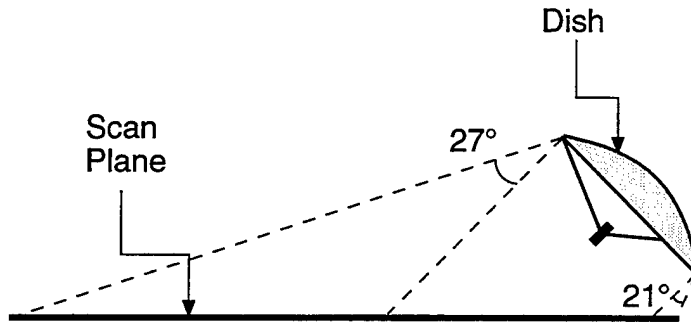


Figure 10: The dish is pointed at an angle of 45 degrees with respect to the normal vector of the scan plane.

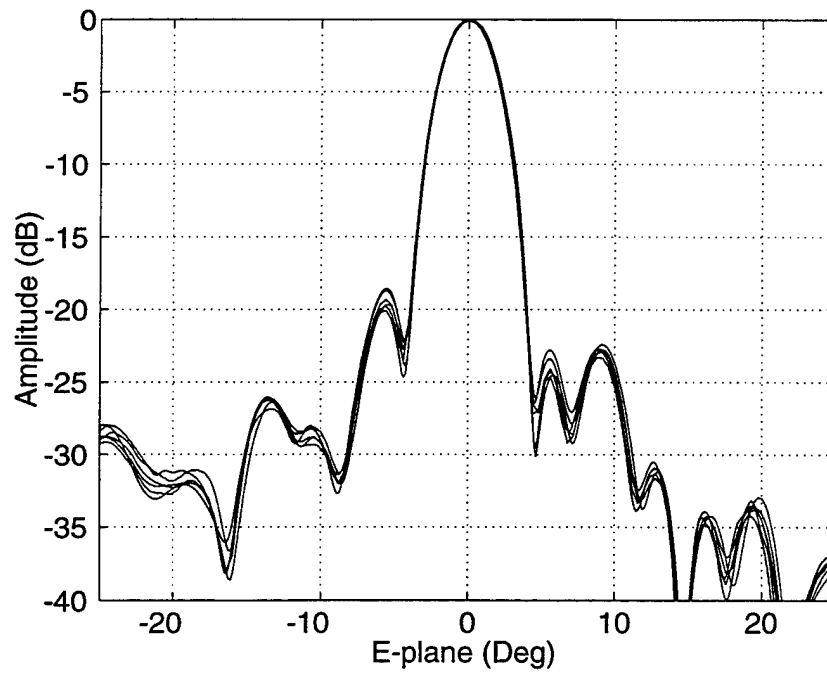


Figure 11: Comparison of E-plane far-zone pattern obtained from the near-field range at 10 GHz using the normal configuration in Figure 3 versus the tilted arrangement in Figure 10.

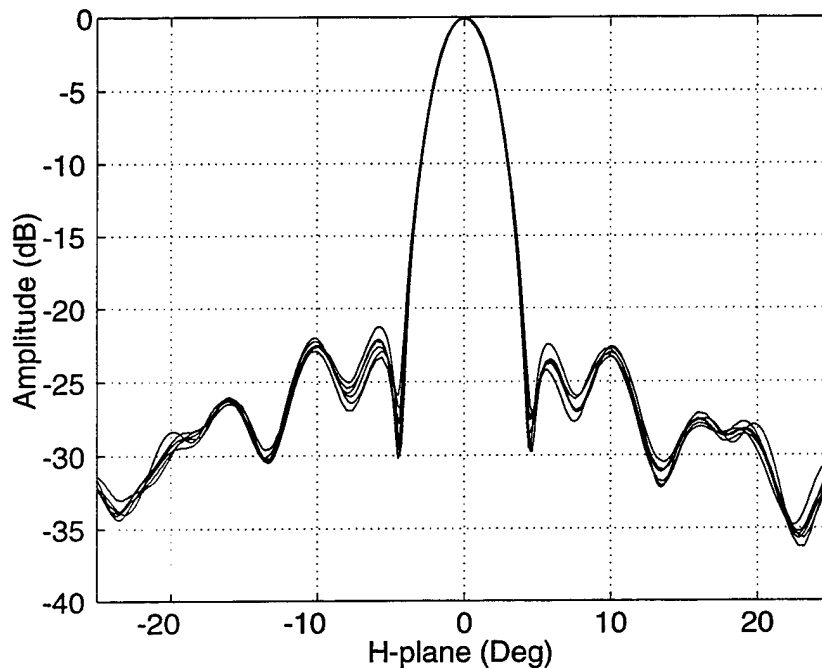


Figure 12: Comparison of H-plane far-zone pattern obtained from the near-field range at 10 GHz using the normal configuration in Figure 3 versus the tilted arrangement in Figure 10.

**Example: Measurement of sidelobe levels far from the main beam direction**

One of the benefits of measuring an antenna that is tilted with respect to the scan plane is the ability to measure the sidelobes far from the boresight direction. In fact, it is possible to measure sidelobes beyond 90 degrees as shown in the following example. Note, however, that it is theoretically impossible to measure sidelobes beyond 90 degrees using a normal configuration, where the AUT boresight is perpendicular to the scan plane, like the one shown in Figure 3.

The near-field range measurement configuration is shown in Figure 13. The GO based rule of thumb predicts that the far-zone patterns obtained from this arrangement will be valid all the way out to 120 degrees on one side. In order to obtain the far off sidelobes on the other side, the dish is rotated 180 degrees about its axis and measured again. Obviously, the far-zone patterns from these two measurements at angles less than 23 degrees should agree when the appropriate change of coordinates is taken into account.

Figures 14 and 15 show a comparison of the far-zone patterns as measured on a far-zone range and the near-field range at 10 GHz. The far-zone patterns from the near-field range are obtained by measuring the dish as shown in Figure 13 and rotating the dish 180 degrees about its axis and measuring it again, as described

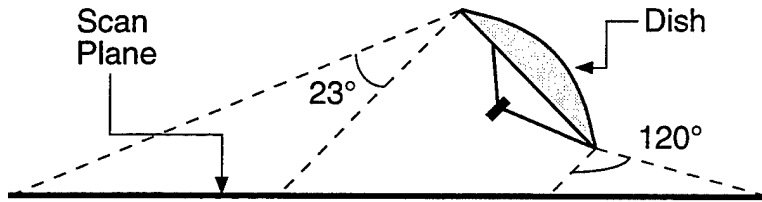


Figure 13: Configuration for measuring the far-sidelobes of the dish. The dish is measured once to obtain the sidelobes out to 120 degrees on one side and then rotated 180 degrees about its axis and measured again to obtain the sidelobes out to 120 degrees on the other side. The dish is tilted 45 degrees with respect to the scan plane.

above. The patterns agree very well all the way out to 120 degrees from the boresight direction. Figures 16 through 21 show similar results for 9, 11 and 12 GHz.

In Figures 14 and 15, there is a small sidelobe at about  $\pm 73$  degrees in the results from the near-field range which does not exist in the far-zone range measurement at 10 GHz. There are similar erroneous sidelobes for the other frequencies as well. These sidelobes are caused by small periodic errors in the lateral probe position. The errors are predicted to be on the order of only 0.003 inches but since the error is periodic and exists throughout the near-field data it causes a grating lobe at a predictable location. This periodic lateral probe position error is caused by the particular raster scan path which is used in these measurements and the construction of the scanner.

It is important to recognize that the lateral probe position errors cause a phase error in the near-field data when the AUT is tilted with respect to the scan plane, but if the AUT is pointed normal to the scan plane then the measurement will be less sensitive to these types of errors.

A simple derivation for the position and magnitude of the erroneous grating lobe is as follows [21]. Consider a two-dimensional scalar near-field measurement for simplicity. The spectrum  $F(k_x)$  (which corresponds directly to the far-zone pattern) is obtained from the near-field  $E(x)$  by a discrete Fourier transform

$$F(k_x) = \sum_{n=1}^N E(x_n) e^{jk_x x_n} \quad (10)$$

where  $x_n$  are the sample point locations and  $k_x = k \sin \theta$ . When the AUT is pointed at an oblique angle  $\theta_0$  with respect to the scan plane the near-field can be approximated by

$$E(x_n) \approx A(x_n) e^{-jk_x x_n \sin \theta_0}$$

where  $A(x_n)$  is a slowly varying function. The periodic  $x$  position error is caused by the particular scan path which is used in the near-field range and can be represented

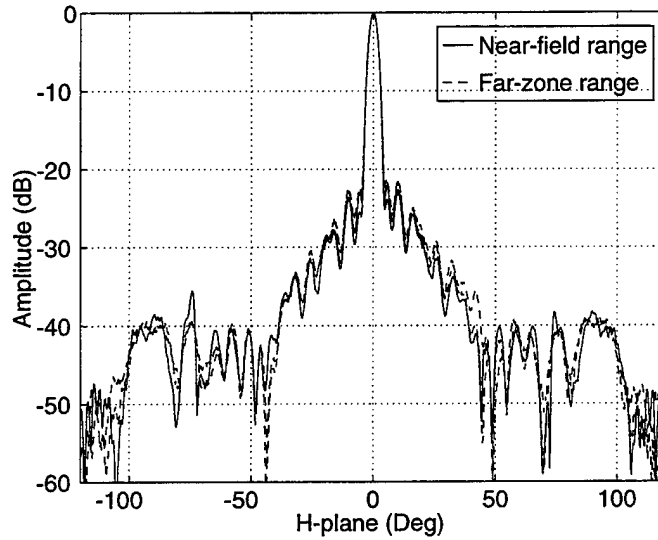


Figure 14: Comparison of H-plane far-zone pattern obtained from near-field range versus the far-zone range at 10 GHz. The near-field range configuration shown in 13 was used in order to measure the sidelobe levels out to 120 degrees off of the boresight direction.

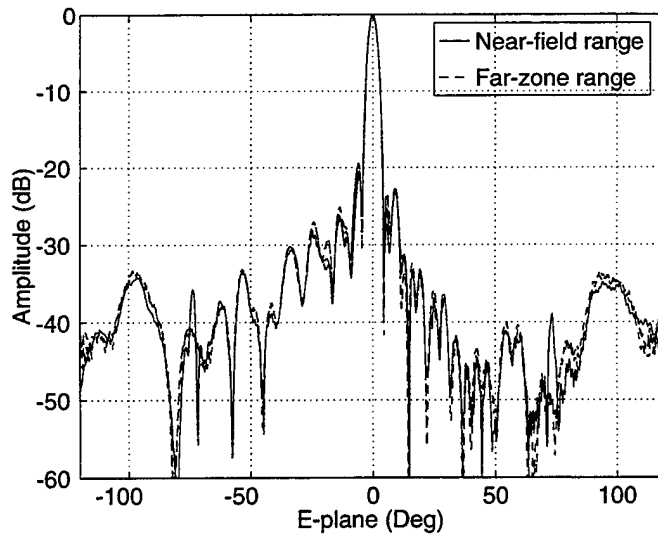


Figure 15: Comparison of E-plane far-zone pattern obtained from near-field range versus the far-zone range at 10 GHz. The near-field range configuration shown in 13 was used in order to measure the sidelobe levels out to 120 degrees off of the boresight direction.



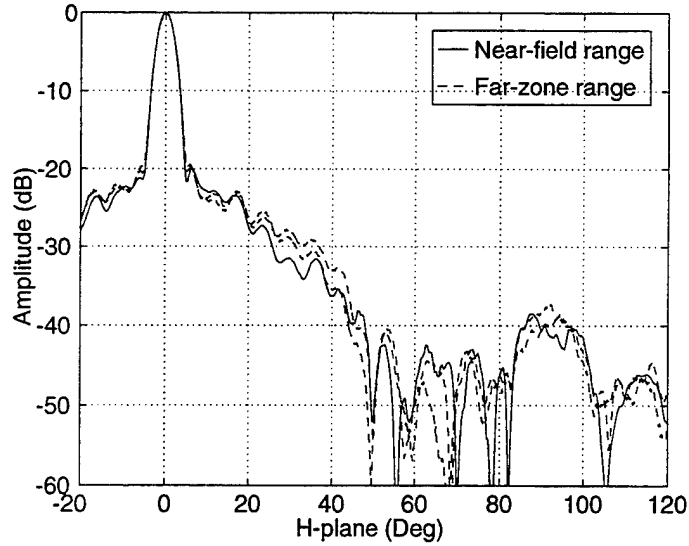


Figure 16: Comparison of H-plane far-zone pattern obtained from near-field range versus the far-zone range at 9 GHz. The near-field range configuration shown in 13 was used in order to measure the sidelobe levels out to 120 degrees off of the boresight direction.

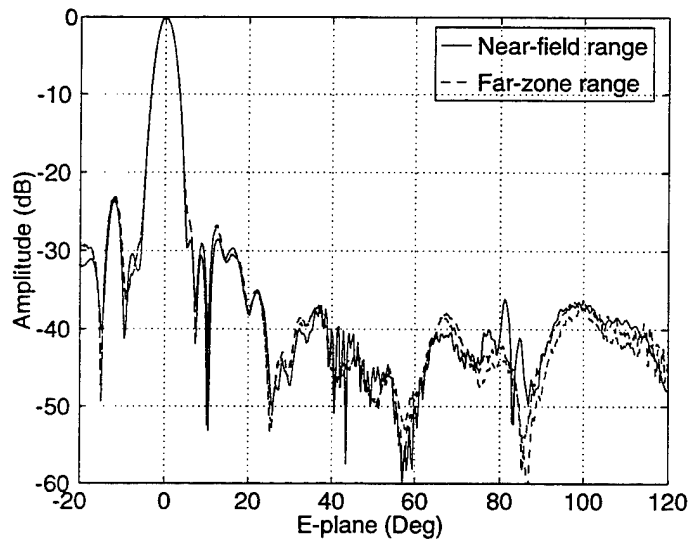


Figure 17: Comparison of E-plane far-zone pattern obtained from near-field range versus the far-zone range at 9 GHz. The near-field range configuration shown in 13 was used in order to measure the sidelobe levels out to 120 degrees off of the boresight direction.

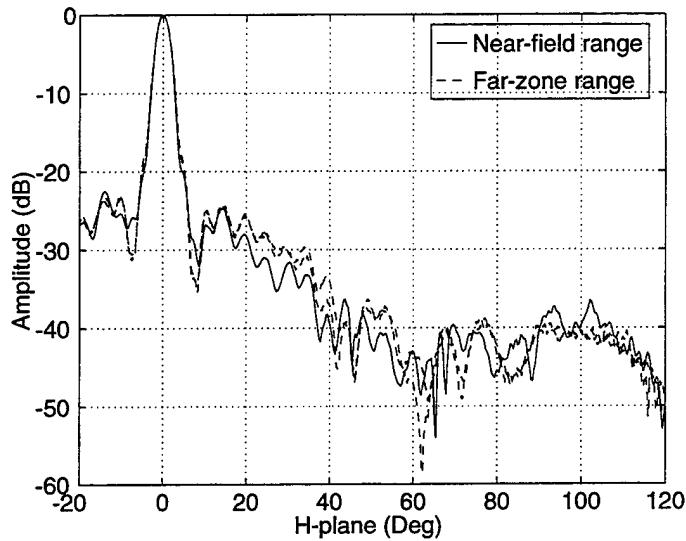


Figure 18: Comparison of H-plane far-zone pattern obtained from near-field range versus the far-zone range at 11 GHz. The near-field range configuration shown in 13 was used in order to measure the sidelobe levels out to 120 degrees off of the boresight direction.

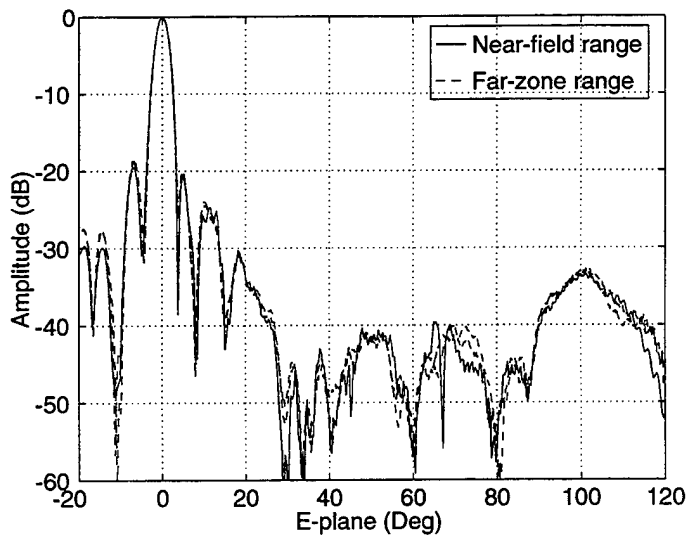


Figure 19: Comparison of E-plane far-zone pattern obtained from near-field range versus the far-zone range at 11 GHz. The near-field range configuration shown in 13 was used in order to measure the sidelobe levels out to 120 degrees off of the boresight direction.

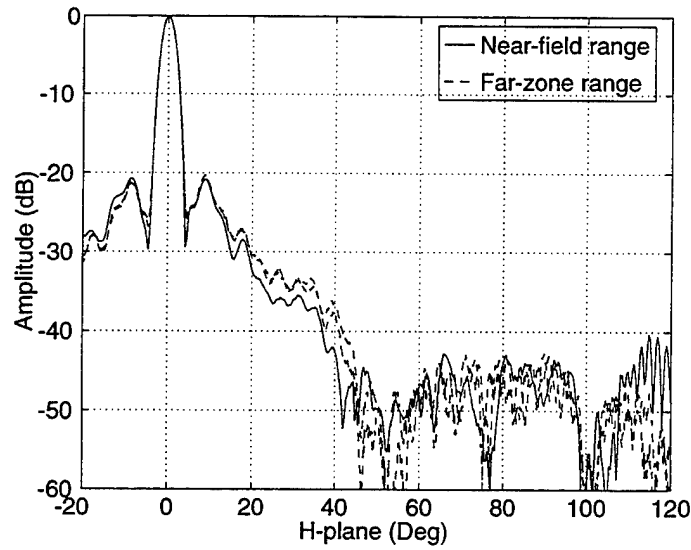


Figure 20: Comparison of H-plane far-zone pattern obtained from near-field range versus the far-zone range at 12 GHz. The near-field range configuration shown in 13 was used in order to measure the sidelobe levels out to 120 degrees off of the boresight direction.

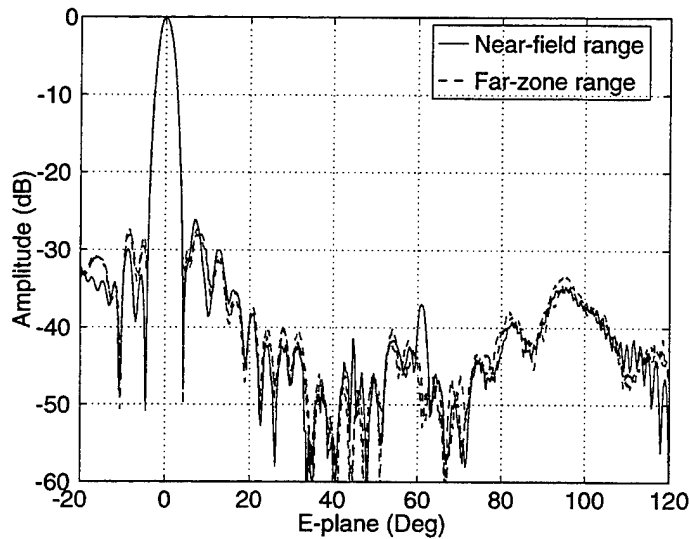


Figure 21: Comparison of E-plane far-zone pattern obtained from near-field range versus the far-zone range at 12 GHz. The near-field range configuration shown in 13 was used in order to measure the sidelobe levels out to 120 degrees off of the boresight direction.

by

$$x_n = x_{on} + \epsilon \cos\left(\frac{2\pi}{2\Delta}x_{on}\right) \quad (11)$$

where the ideal probe position is  $x_{on} = (n-1)\Delta$  and  $\Delta$  is the sample spacing. The cosine function in the above equation simply alternates between a value of +1 and -1 as a function of the index  $n$ . Since  $A(x_n)$  is a slowly varying function, it can be approximated by  $A(x_n) \approx A(x_{on})$ . Now the spectrum is approximated by

$$F(k_x) \approx \sum_{n=1}^N A(x_{on}) e^{jk(\sin\theta - \sin\theta_0)x_{on}} e^{j\alpha \cos(\beta x_{on})} \quad (12)$$

where

$$\alpha = k(\sin\theta - \sin\theta_0)\epsilon \quad (13)$$

$$\beta = \frac{2\pi}{2\Delta} \quad (14)$$

Since the probe position error  $\epsilon$  is small,  $|\alpha| \ll 1$  and

$$e^{j\alpha \cos(\beta x_{on})} \approx 1 + j\frac{\alpha}{2}e^{j\beta x_{on}} + j\frac{\alpha}{2}e^{-j\beta x_{on}} \quad (15)$$

Finally, the spectrum can be written as

$$\begin{aligned} F(k_x) &\approx \sum_{n=1}^N A(x_{on}) e^{jk(\sin\theta - \sin\theta_0)x_{on}} \\ &+ j\frac{\alpha}{2} \sum_{n=1}^N A(x_{on}) e^{jk(\sin\theta - \sin\theta_0 + \beta/k)x_{on}} \\ &+ j\frac{\alpha}{2} \sum_{n=1}^N A(x_{on}) e^{jk(\sin\theta - \sin\theta_0 - \beta/k)x_{on}} \end{aligned} \quad (16)$$

From Equation 16, it is easy to see that there are two possible grating lobes with relative amplitudes of  $\alpha/2$ . The position  $\theta_p$  of the grating lobes caused by the periodic probe position error  $\epsilon$  are

$$\theta_p = \arcsin\left(\sin\theta_0 \pm \frac{\lambda}{2\Delta}\right) \quad (17)$$

where  $\theta_p$  may or may not be real. If  $\theta_p$  is not real then the grating lobe will not appear in the far-zone pattern. From Equation 13, the relative amplitude of the grating lobe at  $\theta_p$  is

$$\frac{\alpha}{2} = 2\pi \frac{\epsilon}{2\Delta} \quad (18)$$

Tables 3 and 4 summarize the location and size of the grating lobe caused by the periodic probe position error as predicted by the above approximations. Notice that the predicted results agree well with the measurements shown in Figures 14 through 21.

Table 3: The relative magnitude of the erroneous grating lobe for various values of probe position error,  $\epsilon$ , when  $\Delta = 0.5$  inches and  $\lambda = 1.18$  inches.

$\epsilon$ (in)	$\alpha/2$ (dB)
0.005	-36
0.002	-44
0.001	-50

Table 4: The relative position of the erroneous grating lobe for various frequencies when  $\theta_0 = -45$  degrees and  $\Delta = 0.5$  inches.

Frequency (GHz)	$\theta_p - \theta_0$ (degrees)
9	82.2
10	73.3
11	66.5
12	61.1

### Example: Coordinate System Convention Confusion

When the AUT is tilted with respect to the scanner there is a potential problem with coordinate system conventions since the near-field data is most naturally processed in the coordinate system of the scanner. Figure 22 shows the AZ-EL coordinate system commonly used to express the far-zone patterns obtained from processing the near-field data [4, 5]. Notice that the Azimuth angle (AZ) in this coordinate system is the negative of that used by Scientific Atlanta [17].

When the principal plane patterns of the AUT are desired, it is common to plot the Azimuth and Elevation patterns which contain the peak of the beam. If the peak of the beam is located close to  $(AZ, EL) = (0, 0)$  then these patterns will closely approximate the principal plane patterns of the AUT. Also, if the peak of the beam is located in the Azimuth plane, say  $(AZ, EL) = (AZ_0, 0)$ , then the Azimuth and Elevation patterns through the peak of the beam will be the principal plane patterns of the AUT. On the other hand, if the peak of the beam is in the Elevation plane, say  $(AZ, EL) = (0, EL_0)$ , then the Elevation pattern will be a principal plane pattern, but the Azimuth pattern will be a conical pattern. This occurs when one uses simple offsets in the Azimuth and Elevation angles to plot the patterns instead of a full coordinate transformation. Some widely used commercial near-field software programs only use offsets and do not perform full coordinate transformations.

Figures 23 and 24 demonstrate the difference between tilting the AUT in the Azimuth plane versus the Elevation plane. The same near-field data was used to generate the far-zone patterns in these figures, only the coordinate system is different.

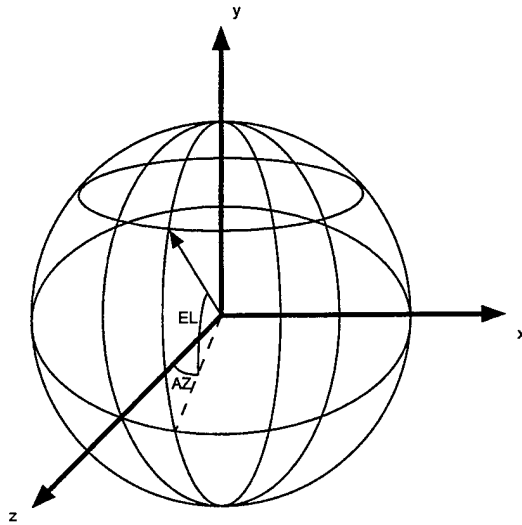


Figure 22: Azimuth-Elevation (AZ-EL) coordinate system used for the far-zone patterns computed from the near-field data. The antenna boresight is in the  $+z$  direction.

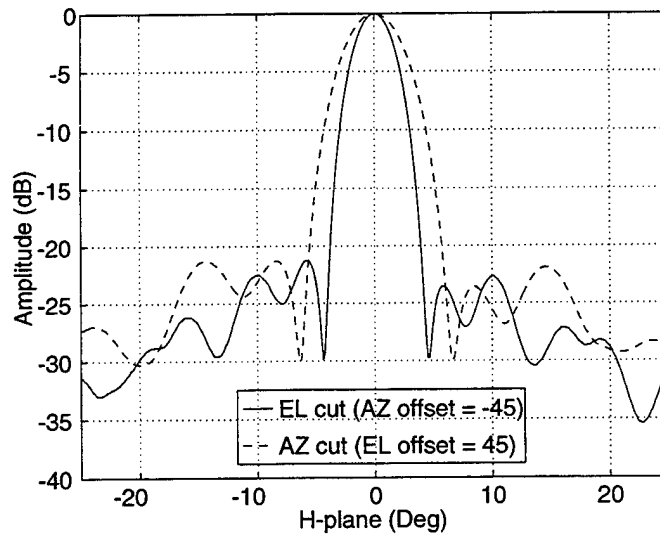


Figure 23: "H-plane" pattern of the two foot dish at 10 GHz. Effect of tilting the AUT in the Azimuth plane versus the Elevation plane. Notice that the Azimuth pattern at a constant Elevation offset (dashed curve) is a conical cut and not a principal plane cut.

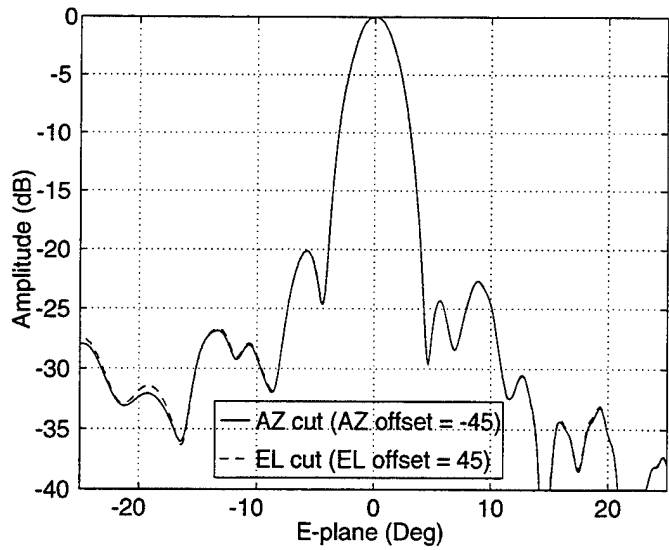


Figure 24: "E-plane" pattern of the two foot dish at 10 GHz. Effect of tilting the AUT in the Azimuth plane versus the Elevation plane.

In the original data, the AUT was tilted in the  $xz$  plane by -45 degrees. For the other case, the data was rotated 90 degrees so that the AUT is effectively tilted by 45 degrees in the  $yz$  plane. Notice that the Azimuth pattern in Figure 23 is a conical pattern instead of a principal plane pattern which is why it does not agree with the other H-plane pattern. In all of the other measurements presented in this paper, the AUT is tilted in the  $xz$  plane or not at all.

## 4 DISH-PLUS-SPLASH-PLATE ANTENNA SYSTEM

The dish-plus-splash-plate antenna system consists of the two foot reflector which was described earlier and a rectangular splash plate as shown in Figure 25. Notice that the splash plate is not perfectly centered on the axis of the dish but is instead offset by 1.2 inches.

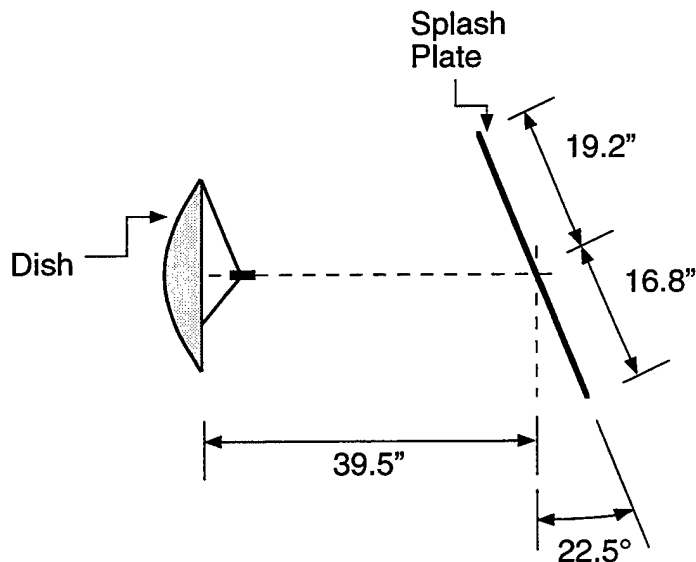


Figure 25: Dish-plus-splash-plate antenna system geometry. The splash plate is rectangular with dimensions of 36 by 26.4 inches.



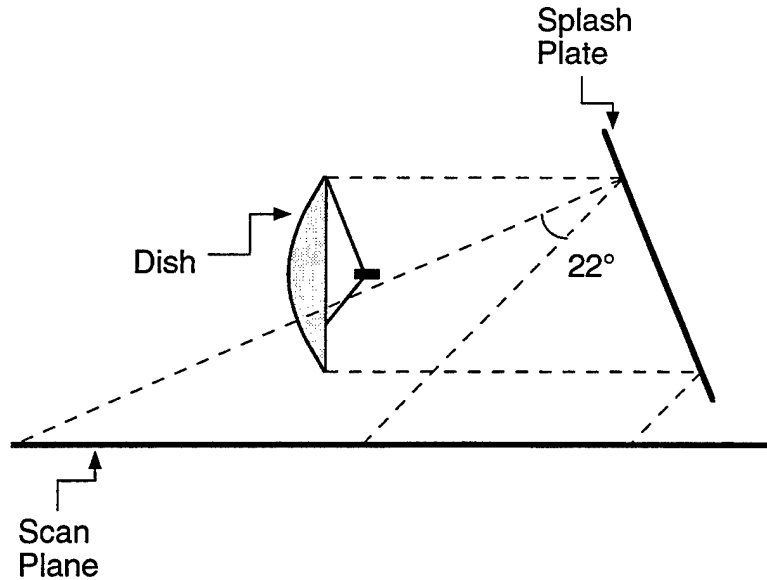


Figure 26: Configuration A for the dish and splash plate.

#### 4.1 Measurement Results of Dish-Plus-Splash-Plate Antenna

The dish-plus-splash-plate antenna was measured in the near-field range in two configurations. In Configuration A, shown in Figure 26, the antenna beam crosses the scan plane at a 45 degree angle and therefore this is a tilted AUT configuration. Notice that the tilt is in the Azimuth plane. Figure 27 shows Configuration B where the antenna beam crosses the scan plane at a 90 degree angle and therefore this is a normal AUT configuration.

The comparison between the far-zone patterns obtained from the near-field range using Configuration A versus Configuration B are shown in Figures 28 through 31. The un-normalized beam peak magnitudes differ by 0.3 dB between Configuration A and Configuration B. This can lead to a difference in measured gain by 0.3 dB between the two configurations. This difference is most likely caused by errors in the probe characterization. Recall that the open ended waveguide (WR90) probe is characterized by simple closed form equations derived by Yaghjian [20].

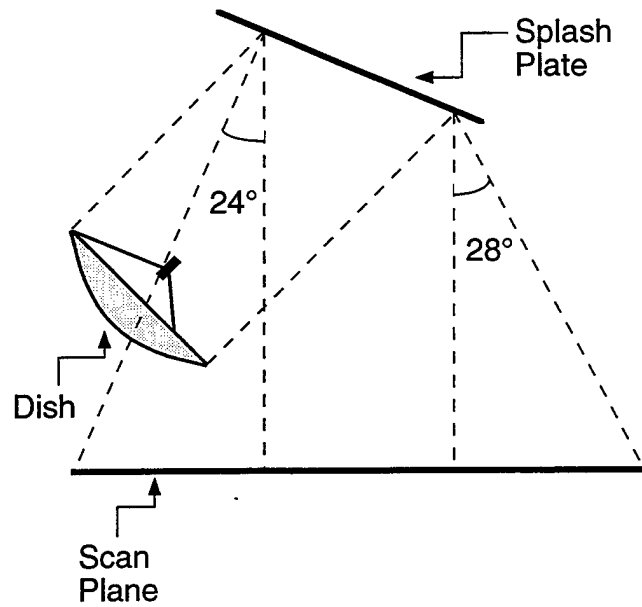


Figure 27: Configuration B for the dish and splash plate.

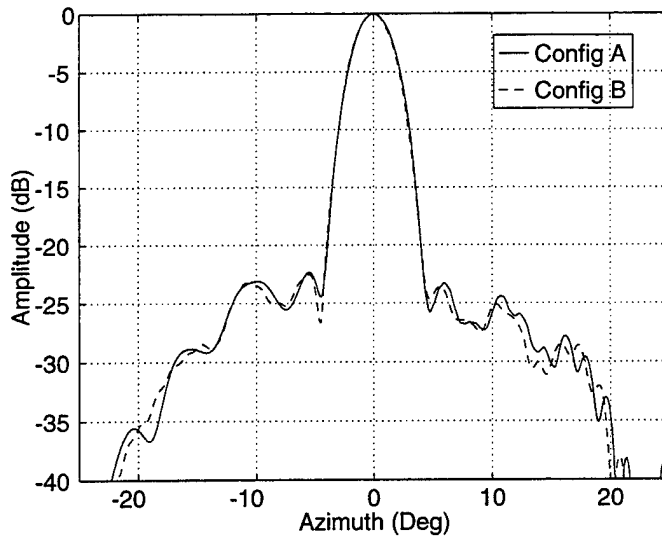


Figure 28: Comparison of the H-plane far-zone pattern at 10 GHz obtained using Configuration B in Figure 27 versus Configuration A in Figure 26. The orientation of the dish is  $\tau = 90$  degrees.

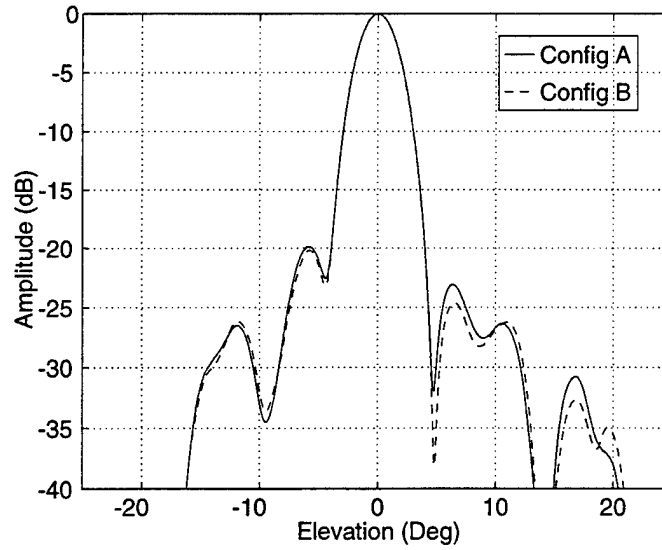


Figure 29: Comparison of the E-plane far-zone pattern at 10 GHz obtained using Configuration B in Figure 27 versus Configuration A in Figure 26. The orientation of the dish is  $\tau = 90$  degrees.

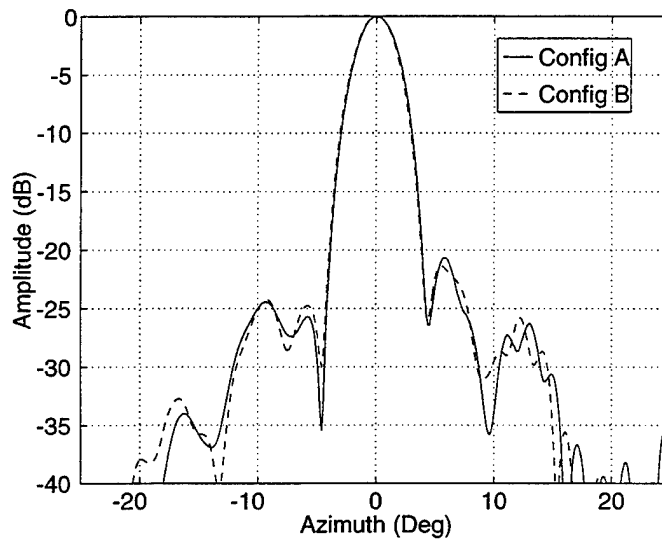


Figure 30: Comparison of the E-plane far-zone pattern at 10 GHz obtained using Configuration B in Figure 27 versus Configuration A in Figure 26. The orientation of the dish is  $\tau = 0$  degrees.

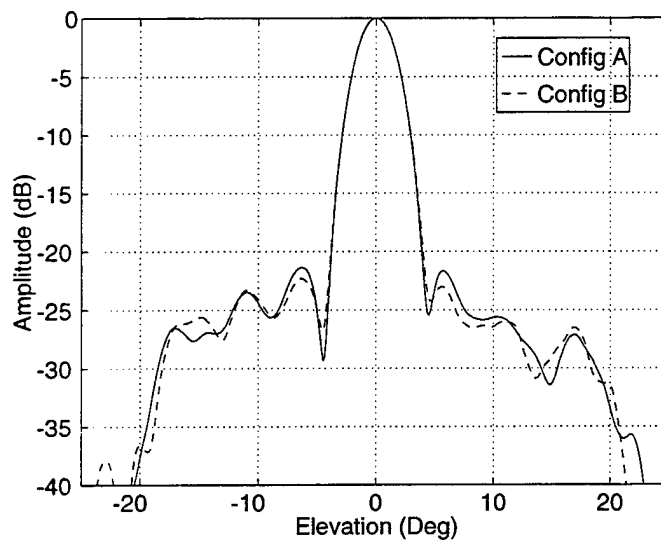


Figure 31: Comparison of the H-plane far-zone pattern at 10 GHz obtained using Configuration B in Figure 27 versus Configuration A in Figure 26. The orientation of the dish is  $\tau = 0$  degrees.

### Example: New Rule of Thumb Demonstration

The rule of thumb based on geometrical optics, presented in Section 3.1.3 and used throughout this paper, is demonstrated by a simple example.

Figure 32 shows the near-field distribution for the dish-plus-splash-plate antenna system measured in Configuration A. To demonstrate the GO based rule of thumb this data is processed three times; once with the original data, once with the data truncated at  $x = -20$  and finally with the data truncated at  $x = -12$ . The data is truncated at  $x = -20$  by setting to zero all of the data points for probe positions with  $x < -20$  and similarly for the  $x = -12$  case. The magnitude of the near-field data at  $x < -20$  is relatively small as seen in Figure 32; down about 40 dB from the peak near-field value. Nonetheless, the GO rule of thumb predicts that the far-zone pattern will not be valid beyond an Azimuth angle of -11 degrees and this can be seen to be true in Figure 33. Table 5 summarizes the predictions of the GO based rule of thumb for this example.

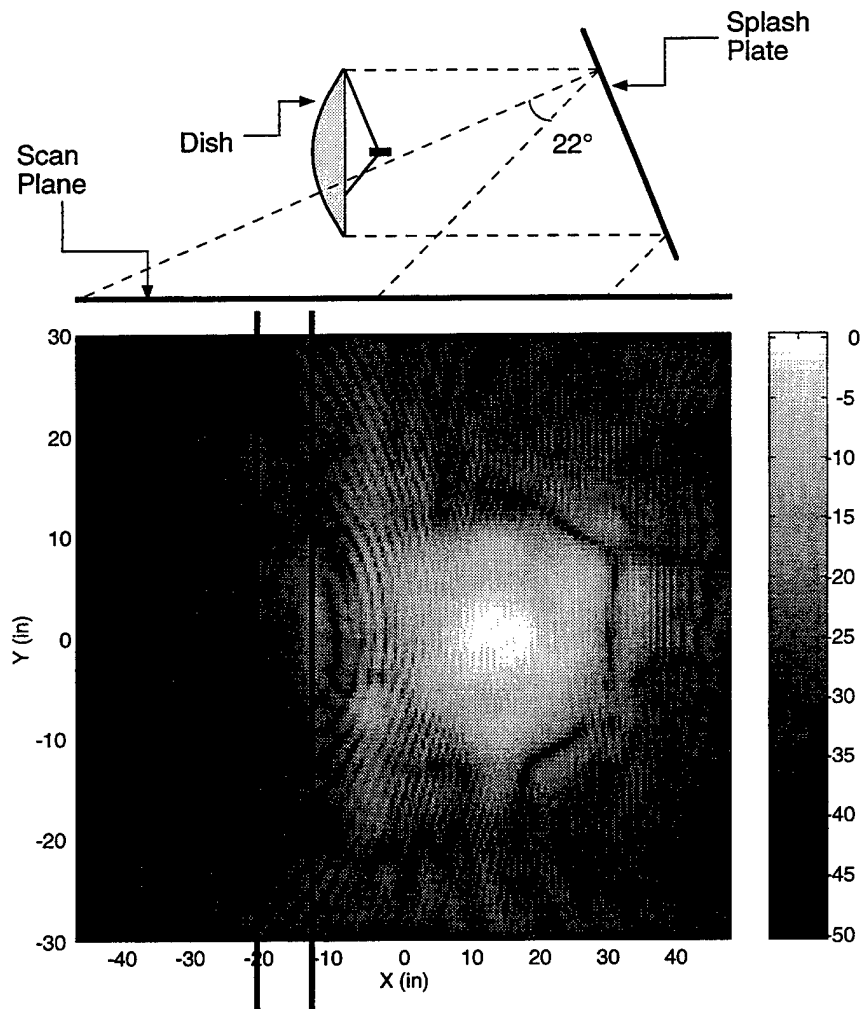


Figure 32: The near-field distribution of the dish-plus-splash-plate antenna system as measured in Configuration A at 10 GHz. This distribution is truncated at  $x = -20$  and  $x = -12$  to examine the usefulness of the new GO based rule of thumb.

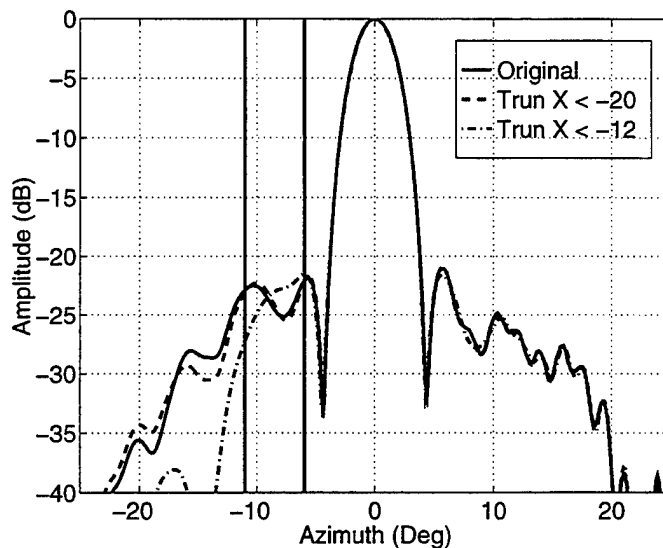


Figure 33: Effect of truncating the near-field data at various  $x$  locations. The GO based rule of thumb predicts the pattern to be valid for  $AZ > -6$  degrees and  $AZ > -11$  degrees when the near-field data is truncated at  $x = -12$  inches and  $x = -20$  inches, respectively.

Table 5: The GO based rule of thumb applied to the measurement in Figures 32 and 33.

Location of $x$ truncation. (inches)	Farthest allowable Azimuth angle predicted by the GO rule of thumb. (degrees)
-48	-22
-20	-11
-12	-6

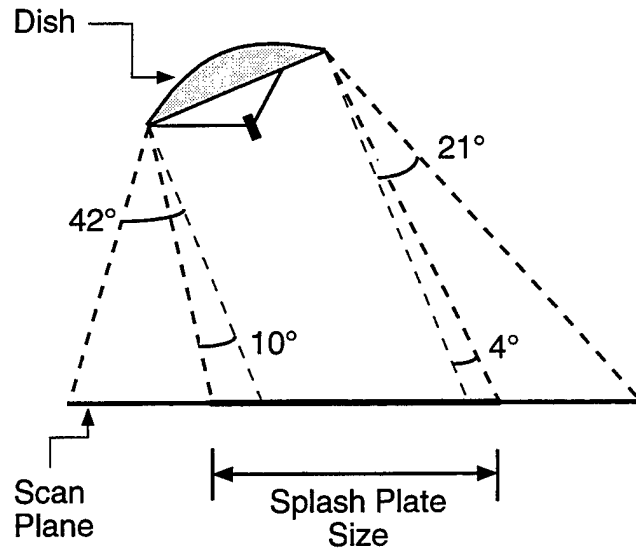


Figure 34: Configuration to measure the dish alone and obtain the electromagnetic fields incident on the splash plate in the dish-plus-splash-plate system. The size of the splash plate is shown as a heavy line in the scan plane. The subtended angles (4 and 10 degrees) in the Azimuth plane for the splash plate are also shown. The subtended angles in the Elevation plane are 31.3 degrees for the full data set and 1.7 degrees for the truncated data set.

### Example: Dish-plus-splash-plate Simulation Using the Measured Fields of the Dish

The far-zone patterns of the dish-plus-splash-plate antenna system can be approximated by computing the scattered field from the splash plate given the incident field from the dish. To measure the fields from the dish incident on the splash plate to the best accuracy, the dish was measured in the arrangement shown in Figure 34. The scan plane is positioned with respect to the dish exactly where the splash plate is positioned in the dish-plus-splash-plate antenna system.

Figure 35 shows the near-field distribution of the dish as measured in the arrangement in Figure 34. To a first order approximation, the fields scattered by the splash plate can be approximated by the far-zone patterns of the dish resulting from a truncation of the near-field distribution shown in Figure 35 to the size of the splash plate. This is very similar to a physical optics calculation, although a more accurate calculation would include a “de-convolution” of the probe response from the measured data before truncation. This simple simulation will obviously not include any higher order interactions between the dish and splash plate which are expected to be significant in the Azimuth patterns. This calculation also does not include the back radiation of the dish which is present in the actual antenna system.



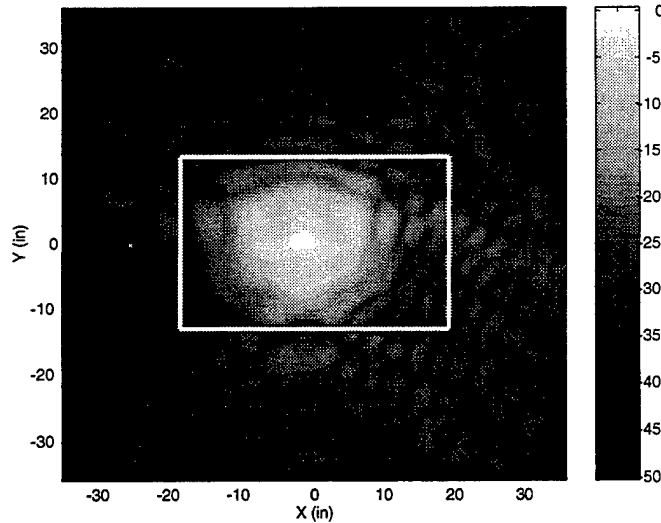


Figure 35: Measured incident field distribution on the splash plate as shown in Figure 34. The frequency is 10 GHz and the polarization is  $\hat{y}$  ( $\tau = 90$ ).

Figures 36 through 39 show a comparison between the patterns of the dish alone using all of the near-field data and the patterns from the truncated data. The dish patterns using the full scan data agree well with the previous measurements in Figures 11 and 12. The main beam peak levels from the full scan data and the truncated scan data agree to within about 0.1 dB, so the gain of a perfect dish-plus-splash-plate antenna system should be very close to the gain of the dish alone.

Figures 40 through 43 show comparisons between the far-zone patterns obtained from simulation versus measurement of the dish-plus-splash-plate system. The simulated patterns are obtained from truncating the measured near-field data of the dish alone to the size of the splash plate as shown in Figures 34 and 35, and the Azimuth patterns are flipped so that the simulation and measured coordinate systems are the same. Two sets of measured data are used for the comparison; one set, labeled “Measured A”, was obtained using Configuration A shown in Figure 26 and the other set, labeled “Measured B” was obtained using Configuration B shown in Figure 27. Some of the small differences between the patterns from Configuration A versus Configuration B are caused by alignment errors between the dish and splash plate. The patterns shown in Figures 40 through 43 are plotted peak relative to each other even though the measurements were taken about one month apart and there is no independent gain calibration. Nonetheless, the peak levels between the measured and simulated results agree to within a couple tenths of a decibel and there is a 0.3 dB systematic difference between the “Measured A” and “Measured B” results. This 0.3 dB difference between the peak levels from Configuration A and Configuration B is most likely caused by probe characterization errors.

It can be seen from Figures 40 through 43 that the simulation is more accurate in

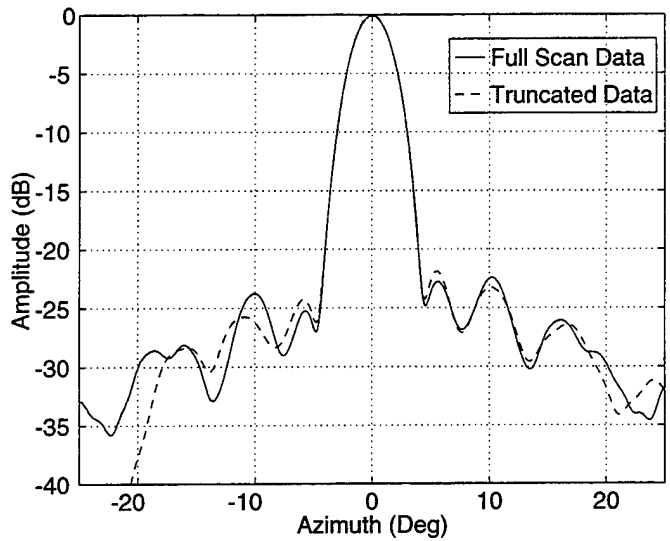


Figure 36: Effect of truncating the near-field data to the size of the splash plate as shown in Figure 35. The near-field range configuration is shown in Figure 34 and the polarization is  $\tau = 90$ .

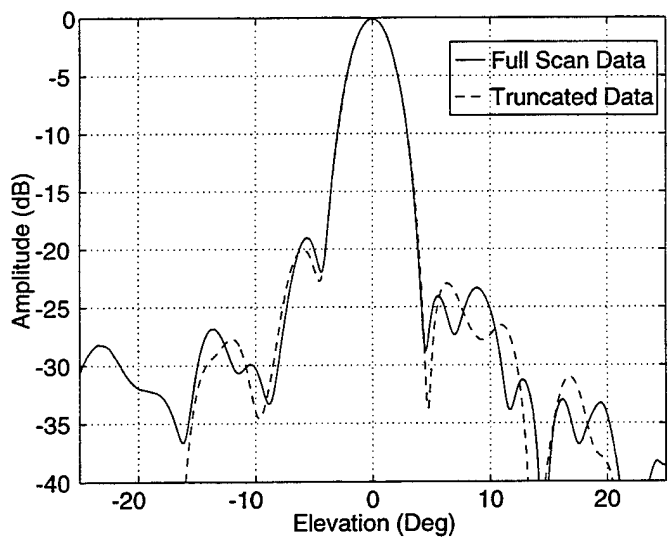


Figure 37: Effect of truncating the near-field data to the size of the splash plate as shown in Figure 35. The near-field range configuration is shown in Figure 34 and the polarization is  $\tau = 90$ .

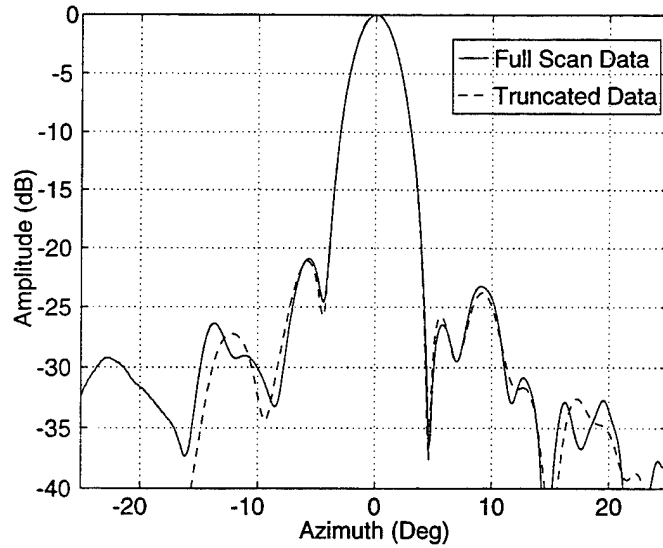


Figure 38: Effect of truncating the near-field data to the size of the splash plate. The near-field range configuration is shown in Figure 34 and the polarization is  $\tau = 0$ .

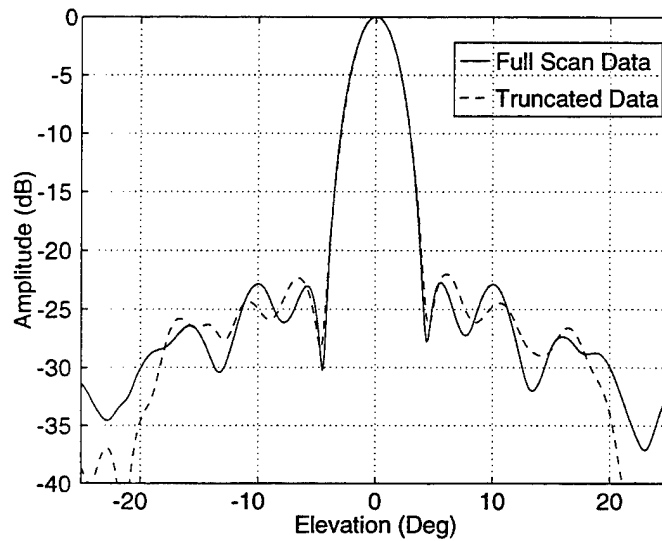


Figure 39: Effect of truncating the near-field data to the size of the splash plate. The near-field range configuration is shown in Figure 34 and the polarization is  $\tau = 0$ .

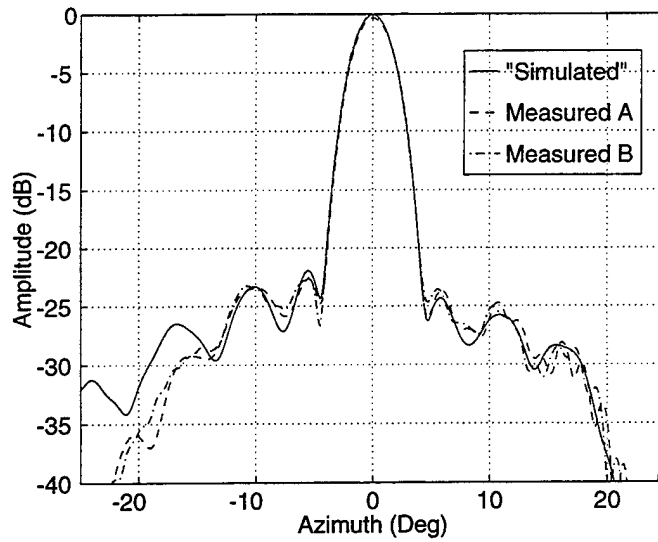


Figure 40: The splash plate is simulated by truncating the measured near-field of the dish alone. The far-zone pattern from this simple simulation is compared with the pattern obtained from measuring the dish-plus-splash-plate system. Measured results using Configuration A (Figure 26) and Configuration B (Figure 27) are shown. The polarization is  $\tau = 90$ .

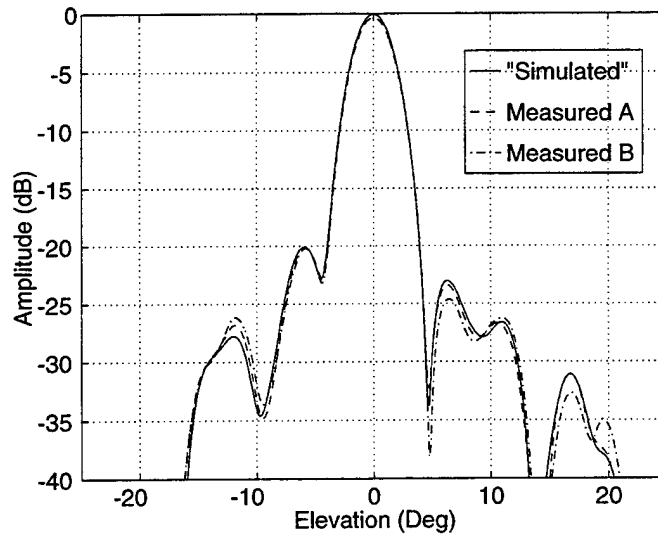


Figure 41: The splash plate is simulated by truncating the measured near-field of the dish alone. The far-zone pattern from this simple simulation is compared with the pattern obtained from measuring the dish-plus-splash-plate system. Measured results using Configuration A (Figure 26) and Configuration B (Figure 27) are shown. The polarization is  $\tau = 90$ .

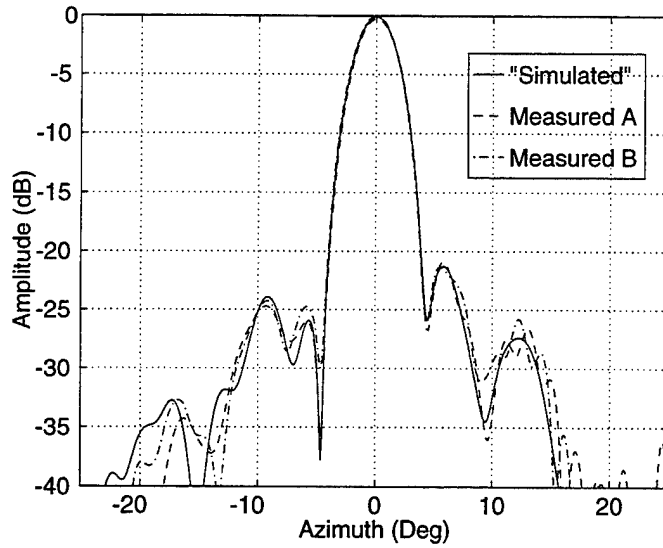


Figure 42: The splash plate is simulated by truncating the measured near-field of the dish alone. The far-zone pattern from this simple simulation is compared with the pattern obtained from measuring the dish-plus-splash-plate system. Measured results using Configuration A (Figure 26) and Configuration B (Figure 27) are shown. The polarization is  $\tau = 0$ .

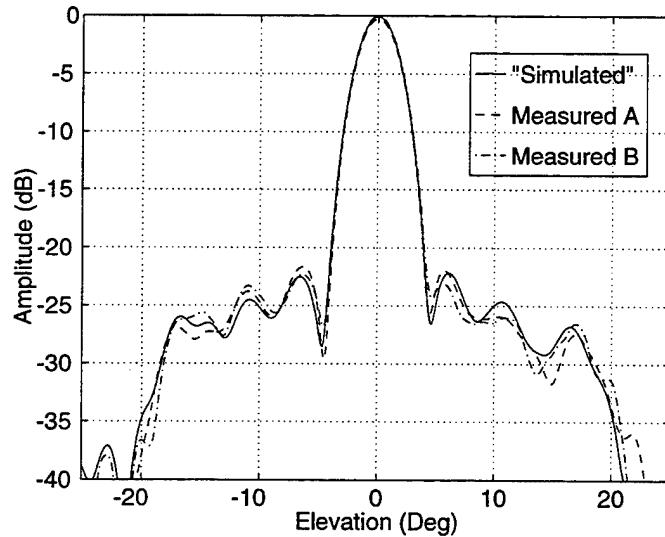


Figure 43: The splash plate is simulated by truncating the measured near-field of the dish alone. The far-zone pattern from this simple simulation is compared with the pattern obtained from measuring the dish-plus-splash-plate system. Measured results using Configuration A (Figure 26) and Configuration B (Figure 27) are shown. The polarization is  $\tau = 0$ .

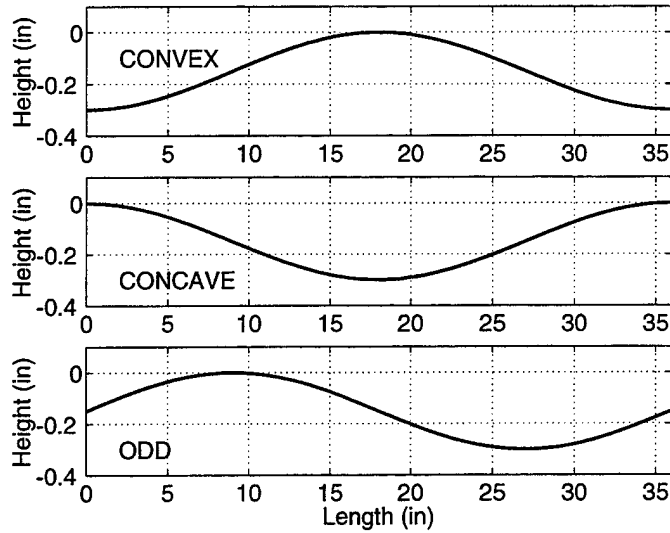


Figure 44: Sketch of the various splash plate deformations. The concave plate is concave when one is looking at the splash plate from the dish's point of view and similarly for the convex plate.

the Elevation patterns than the Azimuth patterns. This is expected since the higher order interactions between the dish and splash plate have a greater effect on the Azimuth patterns rather than the Elevation patterns. As one can see from Figure 26 or 27, the dish will cause a blockage effect for negative angles in the Azimuth pattern and the dish will cause an interference effect for the positive angles in the Azimuth pattern. These effects can be observed in the results shown in Figures 40 through 43.

## 4.2 Splash Plate Deformation Study

This section presents the results from a study of the effects of deterministic deformations of the splash plate on the far-zone patterns of the dish-plus-splash-plate antenna system. Three deformations were studied as shown in Figure 44. The deformations are only in the Azimuth plane and the splash plate was kept flat in the other plane. The plate deformations have a peak to peak variation of 0.3 inches (0.25 wavelengths at 10 GHz).

### 4.2.1 Results

Figures 45 through 47 compare the far-zone Azimuth pattern of the dish-plus-splash-plate antenna with a flat splash plate versus a deformed splash plate. All of the results in this section are at 10 GHz. When the splash plate is deformed, the peak gain level is reduced and the sidelobe levels are higher. In general, there is a degradation of

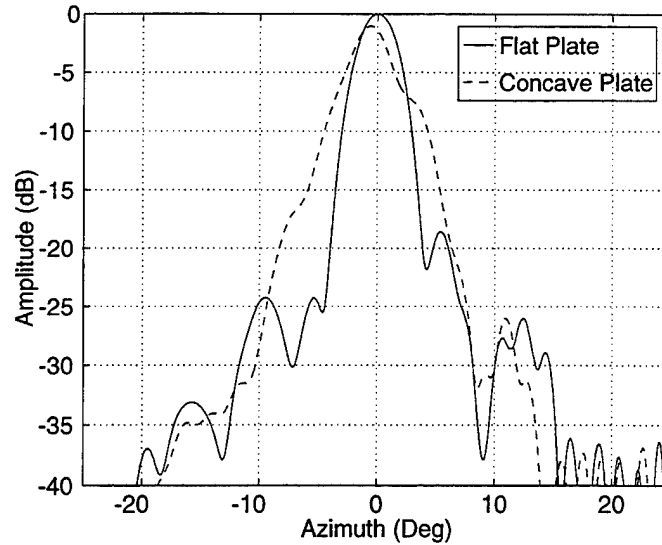


Figure 45: Azimuth pattern of dish-plus-splash-plate antenna with a flat and a concave splash plate. Configuration A in Figure 26 was used and the dish is polarized horizontally or “in the plane of the paper” ( $\tau = 0$ ).

the pattern. Also, there is a squint in the beam direction even for the concave and convex deformations. The squint for the concave and convex deformation cases is caused by the fact the the splash plate is not centered on the axis of the dish, as seen in Figure 25.

To verify that the squints seen in Figures 45 through 47 are caused by the deformations in the splash plate and are not simply a measurement error, a “back of the envelope” approximation of the squint angle is derived by assuming that the squint can be approximated by computing the direction of a geometrical optics ray traveling along the axis of the dish and reflected off of the splash plate. Using this approximation, the predicted squint angles are computed and are summarized in Table 6.

Table 6: Squint errors caused by deformation of the splash plate in the dish-plus-splash-plate antenna system. The measurements referred to here were performed using Configuration A in Figure 26.

Plate	Predicted Squint (Deg)	Measured Squint (Deg)
Flat	0	0 (baseline)
Concave	-0.6	-0.6
Convex	+0.6	+0.5
Odd	-2.9	-2.4

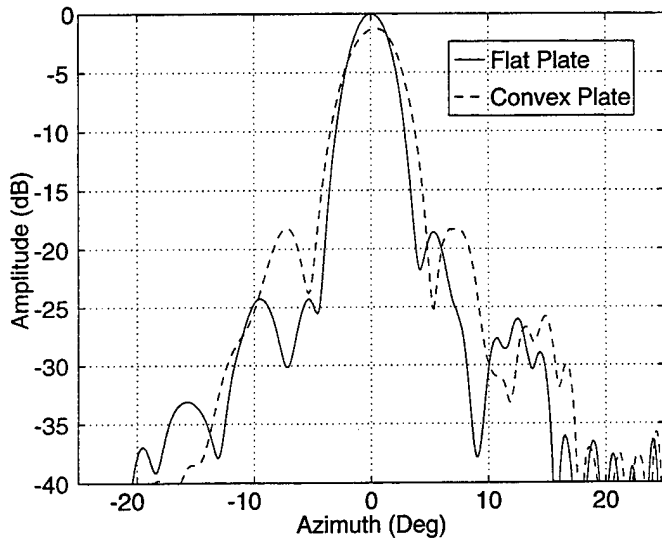


Figure 46: Azimuth pattern of dish-plus-splash-plate antenna with a flat and a convex splash plate. Configuration A in Figure 26 was used and the dish is polarized horizontally or “in the plane of the paper” ( $\tau = 0$ ).

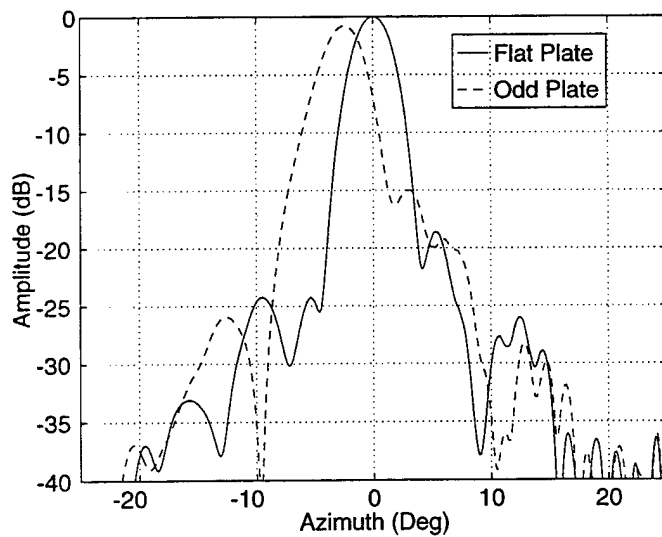


Figure 47: Azimuth pattern of dish-plus-splash-plate antenna with a flat and an odd splash plate. Configuration A in Figure 26 was used and the dish is polarized horizontally or “in the plane of the paper” ( $\tau = 0$ ).





## 5 CONCLUSION

This paper demonstrates the usefulness of measuring an antenna in a tilted configuration in a planar near-field range. A tilted configuration may be necessary for some particular antenna systems which are difficult to align with the scanner, but they are also useful for measuring the sidelobes of the antenna far from the boresight direction and for making self comparison tests to validate the near-field range. The most difficult errors to overcome with a tilted antenna arrangement are those associated with the probe. When the antenna is tilted, the measurement will be more sensitive to lateral probe position errors and also to probe characterization errors. Another issue which must be dealt with is the coordinate system convention used to plot the far-zone patterns of the test antenna. Normally, the coordinate system of the scanner is used but with a tilted configuration the coordinate system of the test antenna is tilted with respect to the scanner. If this tilt is in the Azimuth plane then only a simple Azimuth offset is required, but if this tilt is in the Elevation plane or some other arbitrary direction more care must be exercised.

A simple rule of thumb based on geometrical optics is presented in Section 3.1.3 which relates the antenna and scan plane arrangement to the maximum far-zone angle that can be accurately obtained. Not only is this new rule of thumb useful for setting up a tilted antenna near-field configuration, but it is especially useful for multiple reflector antenna systems.

A dish-plus-splash-plate antenna system is evaluated using the near-field range. Both normal and tilted configurations are used and the results agree well. An investigation of splash plate deformations finds that the far-zone pattern of the antenna system is degraded when the splash plate is deformed as expected. Also, the main beam is squinted in a predictable manner.



## REFERENCES

- [1] A. C. Newell, "Error Analysis Techniques for Planar Near-Field Measurements", *IEEE Trans. Antennas Propagat.*, vol. 36, no. 6, pp. 754-768, Jun. 1988.
- [2] A. D. Yaghjian, "An Overview of Near-Field Antenna Measurements", *IEEE Trans. Antennas Propagat.*, vol. AP-34, no. 1, pp. 30-45, Jan. 1986.
- [3] S. L. Johns, "Analysis and Results of a Splash Plate Scanned Two-Foot Parabolic Reflector Antenna With Struts", ATM 97(8560-02)-1, The Aerospace Corporation, Oct. 1996.
- [4] D. Slater, *Near-field Antenna Measurements*, Artech House, 1991.
- [5] A. C. Newell, *Planar Near-Field Antenna Measurements*, National Institute of Standards and Technology, Mar. 1994, Antenna Parameter Measurements by Near-Field Techniques Short Course.
- [6] J. J. H. Wang, "An Examination of the Theory and Practices of Planar Near-Field Measurement", *IEEE Trans. Antennas Propagat.*, vol. 36, no. 6, pp. 746-753, Jun. 1988.
- [7] D. M. Kerns, "Plane-Wave Scattering Matrix Theory of Antennas and Antenna-Antenna Interactions", NBS Monograph 162, National Bureau of Standards, Jun. 1981.
- [8] A. D. Yaghjian, "Upper-Bound Errors in Far-Field Antenna Parameters Determined From Planar Near-Field Measurements", NBS Technical Note 667, National Bureau of Standards, Oct. 1975.
- [9] A. V. Oppenheim and R. W. Schaffer, *Discrete-Time Signal Processing*, Prentice Hall, Englewood Cliffs, New Jersey, 1989.
- [10] M. H. Francis, A. C. Newell, K. R. Grimm, J. Hoffman, H. E. Schrank, "Comparison of Ultralow-Sidelobe-Antenna Far-Field Patterns Using the Planar-Near-Field Method and the Far-Field Method", *IEEE Ant. and Propag. Magazine*, vol. 37, no. 6, pp. 7-15, Dec. 1995.
- [11] M. H. Francis, A. C. Newell, K. R. Grimm, J. Hoffman and H. E. Schrank, "Planar Near-Field Measurements of Low Sidelobe Antennas", *J. of Research of the National Institute of Standards and Technology*, vol. 99, no. 2, pp. 143-167, Mar.-Apr. 1994.
- [12] M. H. Francis, A. C. Newell, K. R. Grimm, J. Hoffman and H. E. Schrank, "Planar Near-Field Measurements of Low-Sidelobe Antennas", in *AMTA Proceedings*. Antenna Measurements Techniques Association, 1993.

- [13] E. B. Joy, "Near-Field Range Qualification Methodology", *APS*, vol. 36, no. 6, pp. 836–844, Jun. 1988.
- [14] N. Canales, "Planar near-field measurements 1", in *Antenna Parameter Measurements by Near-Field Techniques*. NIST, 1996, Short Course Notes.
- [15] R. C. Johnson, H.A. Ecker and J. H. Hollis, "Determination of Far-Field Antenna Patterns from Near-Field Measurements", *Proc. IEEE*, vol. 61, no. 12, pp. 1668–1694, Dec. 1973.
- [16] D. T. Paris, W. M. Leach Jr. and E. B. Joy, "Basic Theory of Probe-Compensated Near-Field Measurements", *IEEE Trans. Antennas Propagat.*, vol. AP-26, no. 3, pp. 373–389, May 1978.
- [17] J. S. Hollis, T. J. Lyon and L. Clayton, Jr., Ed., *Microwave Antenna Measurements*, Scientific-Atlanta, third edition, 1985, Revised.
- [18] A. G. Repjar, A. C. Newell and M. H. Francis, "Accurate Determination of Planar Near-Field Correction Parameters for Linearly Polarized Probes", *IEEE Trans. Antennas Propagat.*, vol. 36, no. 6, pp. 855–868, Jun. 1988.
- [19] A. C. Newell, C. F. Stubenrauch, "Effect of Random Errors in Planar Near-Field Measurement", *IEEE Trans. Antennas Propagat.*, vol. 36, no. 6, pp. 769–773, Jun. 1988.
- [20] A. D. Yaghjian, "Approximate Formulas for the Far Field and Gain of Open-Ended Rectangular Waveguide", *IEEE Trans. Antennas Propagat.*, vol. AP-32, no. 4, pp. 378–384, Apr. 1984.
- [21] G. E. Stewart, "Lateral Probe Position Error", Private Communication, Sept. 1996.



**THE AEROSPACE  
CORPORATION**

2350 E. El Segundo Boulevard  
El Segundo, California 90245-4691  
U.S.A.